University of Thessaly
School of Engineering
Department of Mechanical Engineering

Thesis

Anisotropic Strain-Gradient Plasticity of Porous Metals

by

SAPOUNAS NIKOLAOS

Diploma in Mechanical Engineering, University of Thessaly, 2019

A Thesis
Submitted in Partial Fulfilment of the
Requirements for the Diploma of
Mechanical Engineer
2019

Approved by the Three Members of the Advisory Committee:

First Member	*Nikolaos Aravas*
(Supervisor)	*Department of Mechanical Engineering, University of Thessaly*
Second Member	*Michalis Agoras*
	Department of Mechanical Engineering, University of Thessaly
Third Member	*Alexis Kermanidis*
	Department of Mechanical Engineering, University of Thessaly

Contents

List of Figures

Chapter 1

Introduction

The present thesis is concerned with the development of a non-local constitutive model for porous metals. The term "non-local" refers to material models in which, e.g., the deformation ε at material point A depends not only on the "local" values of the stress $\boldsymbol{\sigma}$ and the internal variables $\mathbf{q}$ at A , but it depends also on the values of $\boldsymbol{\sigma}$ and $\mathbf{q}$ in the immediate neighborhood of point A. The motivation for the development of these models is twofold. First, we want to develop constitutive models that describe the mechanical behavior of structural metals that account for "material damage" and can be used in the material "softening regime" until final material failure. Second, to introduce "material lengths" that account for the material micro-structure into the constitutive equations. The higher order gradients in the non-local models increase the order of the governing equations and their implementation in commercial finite element programs is not straightforward.
A constitutive model for porous materials was firstly introduced by Gurson [11] and was later altered and improved by various researchers such as Kailasam [14] and Koplik [15]. Gurson's model is an isotropic model for non-hardening metals with dilute porosity levels. Some assumptions made in this model are that the shape of the pores is and remains spherical and secondly, that the load conditions where close to hydrostatic and in order to describe the evolution of the porosity Gurson assumed that the matrix phase will be incompressible. These may at first sound as not some major compromises but in the case of low-triaxiality conditions the model seems to be fairly inaccurate. This can be addressed to the fact that voids do not stay spherical in large amount of plastic deformation.

The non-local model is based on the advanced anisotropic model presented by Ponte Castañeda and co-workers (Kailasam and Ponte Castañeda [13], Aravas and Ponte Castañeda [2]). The model considers the evolution of porosity and the development of anisotropy due to changes in the shape and the orientation of the voids during plastic deformation. At every material point, a "representative" ellipsoid is considered. The basic "internal variables" are the local equivalent plastic strain $\bar{\varepsilon}^p$, the local porosity f_{loc}, the aspect ratios $(w_1 = a_3/a_1, w_2 = a_3/a_2)$ and the orientation of the principal axes $\left(\mathbf{n}^{(1)}, \mathbf{n}^{(2)}, \mathbf{n}^{(3)}\right)$ of the ellipsoid. The material is locally orthotropic with the axes of orthotropy defined by the principal direction of the representative ellipsoid.

We develop a "gradient" version of the model, which is be based on a "non-local" porosity variable f and introduces a "material length" ℓ to the constitutive equations. The non-local

porosity f is defined by an additional boundary value problem (BVP); at a material point P, f can be identified with the average value of the local porosity f_{loc} over a sphere centered at P and of radius approximately equal to $3\,\ell$.
The constitutive model was then implemented in a general-purpose finite element program and the procedure of solving the problem with finite elements in the context of finite strains is presented. The ABAQUS finite element code provides a general interface so that a particular constitutive model can be introduced via a "user subroutine" UMAT (User MATerial).

In Chapter 2 we present the equations regarding plastic behavior, how quantities such as the plastic strain are evolving with respect to time, how porosity is evolving, and how the shape of the pores is alternating.

In Chapter 3 we discuss the numerical implementation of the constitutive model into ABAQUS, a general purpose finite element program.

In Chapter 4 we will verify the results of the model with three-dimensional unit cell calculations. Essentially, these calcultions check the accuracy of the original ***local*** model, as they refer to macroscopically uniform stress fields. Specifically, we consider cubic unit cells with one spherical void in the center.

Finally, in Chapter 5 we summarize the results and make some conclusions, regarding the model used and how it responds according to the stress conditions and porosity levels. At last, there will be some improvements proposed to enhance the model.

Standard notation is used throughout. Boldface symbols denote tensors the orders of which are indicated by the context. All tensor components are written with respect to a fixed Cartesian coordinate system with base vectors $\mathbf{e}_i$ $(i = 1, 2, 3)$, and the summation convention is used for repeated Latin indices, unless otherwise indicated. The prefice det indicates the determinant, a superscript T the transpose, a superposed dot the material time derivative, and the subscripts s and a the symmetric and anti-symmetric parts of a second order tensor. Let $\mathbf{a}$, $\mathbf{b}$ be vectors, $\mathbf{A}$, $\mathbf{B}$ second-order tensors, and $\boldsymbol{\mathcal{C}}$ a fourth-order tensor; the following products are used in the text $(\mathbf{a}\,\mathbf{b})_{ij} = a_i\,b_j$, $\mathbf{A} : \mathbf{B} = A_{ij}\,B_{ij}$, $(\mathbf{A} \cdot \mathbf{B})_{ij} = A_{ik}\,B_{kj}$, $(\mathbf{A}\,\mathbf{B})_{ijkl} = A_{ij}\,B_{kl}$, $(\boldsymbol{\mathcal{C}} : \mathbf{A})_{ij} = \mathcal{C}_{ijkl}\,A_{kl}$, and $(\boldsymbol{\mathcal{C}} : \mathbf{D})_{ijkl} = \mathcal{C}_{ijpq}\,D_{pqkl}$. The inverse $\boldsymbol{\mathcal{C}}^{-1}$ of a fourth-order tensor $\boldsymbol{\mathcal{C}}$ that has the "minor" symmetries $\mathcal{C}_{ijkl} = \mathcal{C}_{jikl} = \mathcal{C}_{ijlk}$ is defined so that $\boldsymbol{\mathcal{C}} : \boldsymbol{\mathcal{C}}^{-1} = \boldsymbol{\mathcal{C}}^{-1} : \boldsymbol{\mathcal{C}} = \boldsymbol{\mathcal{I}}$, where $\boldsymbol{\mathcal{I}}$ is the symmetric fourth-order identity tensor with Cartesian components $\mathcal{I}_{ijkl} = (\delta_{ik}\,\delta_{jl} + \delta_{il}\,\delta_{jk})/2$, δ_{ij} being the Kronecker delta.

Chapter 2

Presentation of the constitutive model for porous materials

2.1 Introduction

In the present thesis we develop a non-local model for porous metals based on the advanced anisotropic model presented by Ponte Castañeda and co-workers (Kailasam and Ponte Castañeda [13], Aravas and Ponte Castañeda [2]). Below some of the basic concepts of the theory are presented.

Porosity

In many incidents of material failure and more especially metal fracture can be observed that one of the main reasons of the failure is the porosity of the metal. Porosity can be measured as the volume fraction of the voids and the total volume of the material. As a number will vary between 0 and 1 and as a percentage between 0-100 percent. The general concept of porosity can be analyzed in 2 kinds. The first kind will be the porosity that the material has by default after its being created. This value will later be described as initial porosity f_0. Initial porosity may result from wrong solidification temperature or rate and gases trapped in the metal material. The typical values of porosity in a stainless steel are between 0-3 percent and the exact maximum for each material is specified by the standard used. The second case of porosity is the nucleation of pores in the material. To better describe this statement, imagine a simple case of axisymmetric elongation. The already existing pores will be stretched, growing in volume but also new pores will be created in random places throughout the material. Here we have to note that void nucleation will be encountered in large deformations.

Distribution of the voids

For porous materials, it was found [8] that the "distribution" effects were small, and it was observed that the approximation of fixing the evolution of the shape and orientation of

the distribution function equal to that of the voids themselves had a small overall effect in the predictions, while greatly simplifying the calculations involved (especially for situations where the distribution ellipsoid and inclusions are not aligned). In this work, use will be made of this simplifying assumption—keeping in mind that it could easily be relaxed at the expense of slightly heavier computation times.

Random orientation

In addition, all the voids will be taken here to have initially the same shape and orientation, even if the general theory [7] can be used to treat the more general case of several families of aligned pores (with different shape and orientation for each family). In particular, the general theory would allow treatment of the case of randomly oriented voids, but this would result in considerable increase in the number of internal variables required, somewhat analogous to the situation for polycrystals, for which a version of the theory has also been developed recently [9].

Original shape of the voids

Thus, the pores will be assumed in this work to be initially ellipsoidal (all with identical shapes and orientations) and distributed randomly (with the same shape and orientation for the distribution as for the voids themselves) in an elastic–plastic matrix (metal). Under finite plastic deformation, the voids remain ellipsoidal but change their volume, shape and orientation with the "local" macroscopic deformation. In this connection, it is emphasized that the size of the voids is assumed to be much smaller than the scale of variation of the macroscopic fields, in such a way that any "representative volume element" of the porous metal deforms uniformly with the local fields.

2.2 Yield condition and plastic flow rule

2.2.1 Definition of yield criterion ($\Phi = 0$)

We study porous elasto-plastic materials. In the plastic region the "history" of deformation cannot be described by a simple function and that created the need to introduce new variables and a new function that, given both the stress and the deformation history of the material, we will acquire the strain. The new variables introduced are called state variables denoted as $\mathbf{s} = \{s_1, s_2, \dots\}$ and are different for each material model. As we previously mentioned, for the anisotropic model we need to define the following set of variables $(\bar{\varepsilon}^p, f_{\text{loc}}, w_1, w_2, \mathbf{n}^{(1)}, \mathbf{n}^{(2)}, \mathbf{n}^{(3)})$. All these constitutive variables are implemented into the yield function of Φ:

$$\Phi(\bar{\varepsilon}^p, f_{\text{loc}}, w_1, w_2, \mathbf{n}^{(1)}, \mathbf{n}^{(2)}, \mathbf{n}^{(3)}) = 0. \tag{2.1}$$

A well-known problem in the computational implementation of damage mechanics models is that finite element solutions depend on the mesh size (i.e., are unreliable), when the material enters the softening region that precedes material failure. The mathematical reason for the mesh dependency is that the governing equations loose ellipticity and the boundary value problem (BVP), as posed originally, becomes ill-conditioned.To overcome this difficulty, it is common to mathematically "regularize" the BVP by introducing in the constitutive equations additional terms that involve higher order spatial gradients of appropriate internal variables. The additional terms in the constitutive equations involve one or more "material lengths" that can be related to material microstructure. The additional gradient terms in the constitutive equations increase the order of the BVP and restore ellipticity, thus leading to reliable mesh-independent numerical solutions, i.e., they regularize the BVP. This regularization has negligible influence on smooth solutions. However, regularization affects substantially local solutions with discontinuities, which are replaced in the non-local solutions by regions of smooth variation with steep spatial gradients; the size of these regions is controlled by the material length and can be related to material microstructure.
Here we develop a gradient version of the anisotropic model, which is be based on a "non-local" porosity variable f and introduces a"material length" ℓ to the constitutive equations. In the present formulation, the ideas of Peerlings et al. [23] and Engelen et al. [8] are used to define the "non-local" field f in terms of the "local" field f_{loc} from the solution of the following boundary value problem:

$$f - \ell^2 \nabla^2 f = f_{\text{loc}} \quad \text{in the domain} \quad \Omega, \tag{2.2}$$

$$\frac{\partial f}{\partial n} = 0 \quad \text{on the boundary} \quad \partial\Omega. \tag{2.3}$$

Now the yield function Φ is of the following form

$$\Phi\left(\boldsymbol{\sigma}, \bar{\varepsilon}^p, f, w_1, w_2, \mathbf{n}^{(1)}, \mathbf{n}^{(2)}, \mathbf{n}^{(3)}\right) = 0. \tag{2.4}$$

2.2.2 Definition of MVAR

Ponte Castañeda [25] introduces an effective yield function Φ and the normalized effective fourth-order viscous compliance tensor $\boldsymbol{m}^{\text{var}}$ that can be written as

$$\boldsymbol{m}^{\text{var}} = \boldsymbol{m}^{\text{var}}(f_{\text{loc}}, w_1, w_2, \mathbf{n}^{(1)}, \mathbf{n}^{(2)}, \mathbf{n}^{(3)}).$$

If we again assume that $\boldsymbol{m}^{\text{var}}$ is based on the non-local porosity, the expression of the new function is

$$\boldsymbol{m}^{\text{var}} = \boldsymbol{m}^{\text{var}}(f, w_1, w_2, \mathbf{n}^{(1)}, \mathbf{n}^{(2)}, \mathbf{n}^{(3)}).$$

An analytical expression for $\boldsymbol{m}^{\text{var}}$ is given in Aravas and Ponte Castañeda [2].

From the paper of Danas and Aravas [7] we can see that the results given from the model with the normal variational linear comparison homogenization method of Ponte Castañeda and Kailasam ([12], [13]) fail to deliver accurate results under high triaxiality. The latest

study [7] is a continuation of the earlier work by Danas and Ponte Castañeda [6] and gives an alternate expression for the m^{var} to produce more accurate predictions for the total rate of change in microstructure and also under large triaxiality conditions.

So m^{var} will be modified to m^{mvar} according to the expression:

$$m^{\text{mvar}} = m^{\text{var}} + (q_{\mathcal{J}}^2 - 1)\, \boldsymbol{\mathcal{J}} : m^{\text{var}} : \boldsymbol{\mathcal{J}},$$

where $\boldsymbol{\mathcal{J}}$ is the fourth-order unit deviatoric tensor and $q_{\mathcal{J}}$ is the correction factor given by the following formula:

$$q_{\mathcal{J}} = \frac{1-f}{\sqrt{f}\ln\frac{1}{f}}.$$

In the paper mentioned above there was made a comparison between the variational bound problem (VAR), the modified variational model (MVAR), the second order model (SOM) and lastly the Gurson model (GUR).
Figure 2.1 shown below was presented in the work of Danas and Aravas [7]. The research was focused on the evolution of the microstructure of porous material under load. More precisely the porosity was set to $f = 1\%$ and the load was axisymmetric with the triaxiality stress being -1 and the "Lode angle" $\theta = 0$.
The purpose of the modification was to give the VAR model the ability to attain the Gurson result in the purely hydrostatic limit.
Starting from a purely deviatoric load and ending with a purely hydrostatic one, the following graph was produced (mentioned in the paper as Figure 3.)
This figure shows the yield surfaces for spherical voids for the models mentioned above where SM is the mean stress and SE is the von Mises stress. As we can see the MVAR comes very close to the solution of the SOM while being close and ending up matching with Gurson's model under SM = 3. Note that the behavior of the non modified model is completely inaccurate with the Gurson of the SOM model.

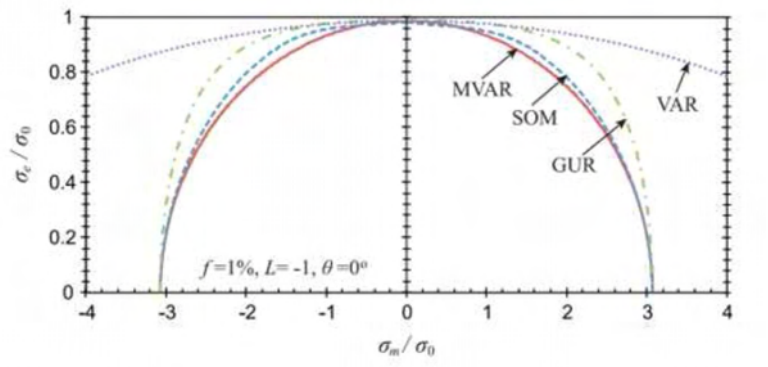

Figure 2.1: Yield surfaces in the $\sigma_e - \sigma_m$ plane for isotropic microstructures. Comparison between the various models (modified variational MVAR, variational VAR, second-order SOM, Gurson GUR) for $f = 1\%$ ans $L = -1$ [7].

2.3 Rate Independent Elastoplasticity

In this section, the *anisotropic* elastic-plastic constitutive model for porous metals is described. The elastic and plastic response of the porous materials are treated independently, and combined later to obtain the full elastic-plastic response. The rate-of-deformation tensor $\mathbf{D}$ at every point in the homogenized porous material is written as

$$\mathbf{D} = \mathbf{D}^e + \mathbf{D}^p, \tag{2.5}$$

where $\mathbf{D}^e$ and $\mathbf{D}^p$ are the elastic and plastic parts.

2.3.1 Equations for the elastic constitutive model

Details on the following equations can be found in the work of Aravas and Ponte Castañeda [2]. We start with the fact that, the hypolelastic corotational constitutive formulation indicates a linear relation between the corotational Cauchy stress rate $\overset{\circ}{\boldsymbol{\sigma}}$ and the elastic part of the deformation rate $\mathbf{D}^e$. The expression is the following:

$$\overset{\circ}{\boldsymbol{\sigma}} = \boldsymbol{\mathcal{L}}^e : \mathbf{D}^e, \tag{2.6}$$

where $\boldsymbol{\mathcal{L}}^e$ is the fourth-order elasticity tensor and $\boldsymbol{\Omega}$ the spin of the local axes of orthotropy. For a small elastic strains it can be proved that

$$\mathbf{W} = \boldsymbol{\Omega} + \mathbf{W}^p. \tag{2.7}$$

The Jaumann derivative $\overset{\triangledown}{\boldsymbol{\sigma}}$ is related to $\overset{\circ}{\boldsymbol{\sigma}}$ by the following expression:

$$\overset{\triangledown}{\boldsymbol{\sigma}} = \overset{\circ}{\boldsymbol{\sigma}} + \boldsymbol{\sigma}\cdot\mathbf{W}^p - \mathbf{W}^p\cdot\boldsymbol{\sigma} = \boldsymbol{\mathcal{L}}^e : \mathbf{D}^e + \boldsymbol{\sigma}\cdot\mathbf{W}^p - \mathbf{W}^p\cdot\boldsymbol{\sigma}. \tag{2.8}$$

We use the Jaumann derivative to ensure the objectivity of the constitutive equations. We will start by the elasticity tensor $\boldsymbol{\mathcal{L}}$ of the matrix material

$$\boldsymbol{\mathcal{L}} = 2\,\mu\,\boldsymbol{\mathcal{K}} + 3\,k\,\boldsymbol{\mathcal{J}}.$$

The elastic compliance tensor $\boldsymbol{\mathcal{M}}$ of the matrix is defined as the inverse of $\boldsymbol{\mathcal{L}}$:

$$\boldsymbol{\mathcal{M}} = \boldsymbol{\mathcal{L}}^{-1} = \frac{1}{2\,\mu}\,\boldsymbol{\mathcal{K}} + \frac{1}{3\,\kappa}\,\boldsymbol{\mathcal{J}} = \frac{1}{2\,\mu}\left(\boldsymbol{\mathcal{K}} + \frac{1-2\,\nu}{1+\nu}\boldsymbol{\mathcal{J}}\right), \tag{2.9}$$

where (μ, κ) is the matrix elastic shear and bulk moduli, ν the matrix Poisson ratio, $\boldsymbol{\mathcal{J}} = \frac{1}{3}\,\boldsymbol{\delta}\,\boldsymbol{\delta}$, $\boldsymbol{\mathcal{K}} = \boldsymbol{\mathcal{I}} - \boldsymbol{\mathcal{J}}$, $\boldsymbol{\mathcal{Q}} = \boldsymbol{\mathcal{L}} : (\boldsymbol{\mathcal{I}} - \boldsymbol{\mathcal{S}})$, and $\boldsymbol{\mathcal{S}}$ is the Eshelby tensor. Note that $\boldsymbol{\mathcal{S}}$ depends on the Poisson ratio ν of the matrix, the aspect ratios of the ellipsoid (w_1, w_2) and the orientation vectors $(\mathbf{n}^{(1)}, \mathbf{n}^{(2)}, \mathbf{n}^{(3)})$. The fourth-order tensor $\boldsymbol{\mathcal{Q}}$ is linearly dependent on the shear modulus μ of the matrix and also depends on Poisson ratio ν, the aspect ratios and the orientation vectors.

We can write equation (2.6) as:

$$\mathbf{D}^e = \boldsymbol{\mathcal{M}}^e : \overset{\circ}{\boldsymbol{\sigma}},$$

where

$$\boldsymbol{\mathcal{M}}^e = (\boldsymbol{\mathcal{L}}^e)^{-1} = \boldsymbol{\mathcal{M}} + \frac{f}{1-f}\boldsymbol{\mathcal{Q}}^{-1}.$$

2.3.2 Equations for the plastic constitutive model

We continue with the constitutive equations for the plastic part of the material behaviour that will be based on the works of Ponte Castañeda [25] and Ponte Castañeda and Willis [26]. The yield function Φ of the porous medium is of the form:

$$\Phi(\boldsymbol{\sigma}, f, w_1, w_2, \mathbf{n}^{(1)}, \mathbf{n}^{(2)}, \mathbf{n}^{(3)}) = \sqrt{\frac{\boldsymbol{\sigma} : \boldsymbol{m}^{\text{var}} : \boldsymbol{\sigma}}{1-f}} - \sigma_y(\bar{\varepsilon}^p), \tag{2.10}$$

where $\sigma_y(\bar{\varepsilon}^p)$ is the yield stress of the matrix material. As we can see the expression of the yield function includes the modified tensor $\boldsymbol{m}^{\text{var}}$ mentioned above and is expressed with respect to the non-local porosity.
The expression of the plastic part of deformation can be expressed in terms of Φ from the "normality" relation:

$$\mathbf{D}^p = \dot{\lambda}\,\mathbf{N}, \qquad \mathbf{N} = \frac{\partial \Phi}{\partial \boldsymbol{\sigma}}, \tag{2.11}$$

where $\dot{\lambda} \geq 0$ is the "plastic multiplier". In the local version of the model, the implicit expression of the plastic multiplier can be calculated according to Dafalias [5] as:

$$\dot{\lambda} = \frac{1}{L}\mathbf{N} : \boldsymbol{\mathcal{L}}^e : \mathbf{D}, \tag{2.12}$$

where H is the "hardening modulus" and L is given by the following formula:

$$L = H + \mathbf{N} : \boldsymbol{\mathcal{L}}^e : \mathbf{N}.$$

In the non-local version, as we will see in section 2.6, λ is calculated

$$\dot{\lambda} = \frac{1}{L}\left(\mathbf{N} : \boldsymbol{\mathcal{L}}^e : \mathbf{D} + \frac{\partial \Phi}{\partial f}\dot{f}\right). \tag{2.13}$$

In the case where the voids are assumed to be spherical and both the aspect ratios are equal to 1 we can safely assume that the material is isotropic and the yield function takes the form:

$$\Phi(\boldsymbol{\sigma}, \bar{\varepsilon}^p, f) = \frac{1}{1-f}\sqrt{\left(1 + \frac{2}{3}f\right)\sigma_e^2 + \frac{9}{4}f\,p^2} - \sigma_y(\bar{\varepsilon}^p) = 0. \tag{2.14}$$

The "hardening modulus" will later be used in section 2.6 along with the Jaumann rate formulation of hypoelasticity.

2.4 Evolution of the equivalent plastic strain $\bar{\varepsilon}^p$ and the local porosity f_{loc}

When the porous material deforms plastically, the state variables evolve and, in turn, influence the response of the material. In the current application to porous metals, it is assumed that all the changes in the microstructure occur only due to the plastic deformation of the matrix, which changes the volume, the shape and the orientation of the voids. In this

section, we are going to focus on the equivalent plastic strain $\bar{\varepsilon}^p$ and the local porosity f_{loc}.

In the classical formulation, considering the physics of the problem, one can derive the evolution equation of the equivalent plastic strain $\bar{\varepsilon}^p$ by postulating that the local "macroscopic" plastic work $\boldsymbol{\sigma} : \mathbf{D}^p = \dot{\lambda}\,\boldsymbol{\sigma} : \mathbf{N}$ equals the corresponding "microscopic" work $(1-f)\,\sigma_y\,\dot{\bar{\varepsilon}}^p$, i.e.,

$$\dot{\bar{\varepsilon}}^p = \dot{\lambda}\,\frac{\boldsymbol{\sigma} : \mathbf{N}}{(1-f)\,\sigma_y(\bar{\varepsilon}^p)}\,. \tag{2.15}$$

We now continue with evolution equation for the local porosity f_{loc}. As said before local porosity is the fraction between the volume of the pores and the total volume of the material in the localized problem

$$f_{\text{loc}} = \frac{V_{\text{por}}}{V}.$$

So we derive

$$\dot{f}_{\text{loc}} = \frac{\dot{V}_{\text{por}}}{V} - \frac{V_{\text{por}}}{V^2}.$$

If we then assume that the rate of volume growth is a result of the pores enlarging $\dot{V}_{\text{por}} = \dot{V}$ then:

$$\dot{f}_{\text{loc}} = \frac{\dot{V}}{V} - f_{\text{loc}}\frac{\dot{V}}{V} = (1-f_{\text{loc}})\frac{\dot{V}}{V}.$$

From the theory of Continuum Mechanics we know that the expression between the initial and the final volume can be expressed with the help of the $J = \det\mathbf{F}$ as $dV = J\,dV_0$, where $\mathbf{F}$ is the deformation gradient. Then

$$dV = J\,dV_0 \quad \Rightarrow \quad d\dot{V} = \dot{J}\,dV_0 \quad \Rightarrow \quad d\dot{V} = J\,D_{kk}\,dV_0 \quad \Rightarrow \quad \frac{\dot{V}}{V} = D_{kk}.$$

The rate of local porosity can be now expressed as

$$\dot{f}_{\text{loc}} = (1-f_{\text{loc}})\,D^p_{kk}, \tag{2.16}$$

where D^p_{kk} is the plastic part of the volumetric deformation rate.
As we said in the beginning where we were explaining the concept of porosity $\dot{f}_{\text{loc}}$ can be divided in the pores that already exist and nucleation of new pores.
If new voids are nucleated during plastic flow by cracking or interfacial decohesion of inclusion or precipitate particles, Chu and Needleman [20] proposed the following expression for the nucleating pores:

$$\dot{f}^{\text{nucl}}_{\text{loc}} = \mathrm{T}(\bar{\varepsilon}^p)\,\dot{\bar{\varepsilon}}^p, \tag{2.17}$$

where

$$\mathrm{T}(\bar{\varepsilon}^p) = \frac{f_N}{s_N\sqrt{2\,\pi}}\exp\left[-\frac{1}{2}\left(\frac{\bar{\varepsilon}^p - \varepsilon_N}{s_N}\right)^2\right].$$

So the evolution equation of the local porocity takes the following form:

$$\dot{f}_{\text{loc}} = \dot{f}^{\text{growth}}_{\text{loc}} + \dot{f}^{\text{nucl}}_{\text{loc}} = (1-f)\,D^p_{kk} + \mathrm{T}(\bar{\varepsilon}^p)\,\dot{\bar{\varepsilon}}^p = \dot{\lambda}\,\left[(1-f)\,N_{kk} + \mathrm{T}\frac{\boldsymbol{\sigma} : \mathbf{N}}{(1-f)\,\sigma_y(\bar{\varepsilon}^p)}\right]. \tag{2.18}$$

2.5 Evolution of the local aspect ratios and the local axes of orthotropy

Ponte Castañeda and co-workers ([25],[13]) have proven that the deformation rate $\mathbf{D}^v$ and the average spin $\mathbf{W}^v$ in the local representative ellipsoidal void are

$$\mathbf{D}^v = \boldsymbol{\mathcal{A}} : \mathbf{D}^p \tag{2.19}$$

and

$$\mathbf{W}^v = \mathbf{W} - \boldsymbol{\mathcal{C}} : \mathbf{D}^p, \tag{2.20}$$

where $\boldsymbol{\mathcal{A}}$ is the fourth order deformation "concentration" tensor and $\boldsymbol{\mathcal{C}}$ is the fourth order spin"concentration tensor" of the vacuum phase. $\boldsymbol{\mathcal{A}}$ and $\boldsymbol{\mathcal{C}}$ are given by the formula:

$$\boldsymbol{\mathcal{C}} = -(1 - f_{\text{loc}})\boldsymbol{\Pi} : \boldsymbol{\mathcal{A}}$$

and

$$\boldsymbol{\mathcal{A}} = [\boldsymbol{\mathcal{I}} - (1 - f_{\text{loc}})\, \boldsymbol{\mathcal{S}}|_{\nu=1/2}]^{-1},$$

where $\boldsymbol{\Pi}$ is the forth order rotation Eshelby tensor described extensively in [9] and [10].
The evolution of the aspect ratios (w_1, w_2) is determined as follows. Starting with the definition:

$$w_1 = \frac{a_3}{a_1}$$

we have:

$$\dot{w}_1 = \frac{\dot{a}_3\, a_1 - a_3\, \dot{a}_1}{a_1^2} = \frac{a_3}{a_1}\frac{a_1}{a_3}\left(\frac{\dot{a}_3}{a_1} - \frac{a_3\, \dot{a}_1}{a_1^2}\right) = w_1\left(\frac{\dot{a}_3}{a_3} - \frac{\dot{a}_1}{a_1}\right). \tag{2.21}$$

Taking into account that

$$\mathbf{n} \cdot \mathbf{D} \cdot \mathbf{n} = D_{nn} = \frac{\dot{\lambda}}{\lambda},$$

we derive

$$\dot{w}_1 = w_1(\mathbf{n}^{(3)}\cdot\mathbf{D}^v\cdot\mathbf{n}^{(3)} - \mathbf{n}^{(1)}\cdot\mathbf{D}\cdot\mathbf{n}^{(1)}) = w_1(\mathbf{n}^{(3)}\mathbf{n}^{(3)} - \mathbf{n}^{(1)}\mathbf{n}^{(1)}) : \mathbf{D}^v = \dot{\lambda}\, w_1(\mathbf{n}^{(3)}\mathbf{n}^{(3)} - \mathbf{n}^{(1)}\mathbf{n}^{(1)}) : \mathcal{A} : \mathbf{N}$$

or

$$\dot{w}_1 = \dot{\lambda}\, g_2(\boldsymbol{\sigma}, f, w_1, w_2, \mathbf{n}^{(1)}, \mathbf{n}^{(2)}, \mathbf{n}^{(3)}). \tag{2.22}$$

Similarly

$$\dot{w}_2 = w_2(\mathbf{n}^{(3)}\cdot\mathbf{D}^v\cdot\mathbf{n}^{(3)} - \mathbf{n}^{(2)}\cdot\mathbf{D}\cdot\mathbf{n}^{(2)}) = w_1(\mathbf{n}^{(3)}\mathbf{n}^{(3)} - \mathbf{n}^{(2)}\mathbf{n}^{(2)}) : \mathbf{D}^v = \dot{\lambda}\, w_2(\mathbf{n}^{(3)}\mathbf{n}^{(3)} - \mathbf{n}^{(2)}\mathbf{n}^{(2)}) : \mathcal{A} : \mathbf{N}$$

or

$$\dot{w}_2 = \dot{\lambda}\, g_3(\boldsymbol{\sigma}, f, w_1, w_2, \mathbf{n}^{(1)}, \mathbf{n}^{(2)}, \mathbf{n}^{(3)}). \tag{2.23}$$

2.6 Rate form of the elastoplastic equations

In order to correctly develop the constitutive equations we need an equation relating the Jaumann derivative of the stress tensor $\overset{\triangledown}{\boldsymbol{\sigma}}$ to the total deformation rate $\mathbf{D}$.
Assuming plastic loading $\dot{\lambda} \geq 0$, substitution of

$$\mathbf{D}^e = \mathbf{D} - \mathbf{D}^p = \mathbf{D} - \dot{\lambda}\,\mathbf{N}$$

into

$$\mathbf{D}^e = \boldsymbol{\mathcal{M}}^e : \overset{\circ}{\boldsymbol{\sigma}}$$

yields

$$\overset{\circ}{\boldsymbol{\sigma}} = \boldsymbol{\mathcal{L}}^e : \mathbf{D} - \dot{\lambda}\,\boldsymbol{\mathcal{L}}^e : \mathbf{N}, \tag{2.24}$$

where $\boldsymbol{\mathcal{L}}^e = (\boldsymbol{\mathcal{M}}^e)^{-1}$. Since Φ is an isotropic function, the "consistency condition" $\dot{\Phi} = 0$ according to [2] can be written in the form

$$\dot{\Phi} = \frac{\partial \Phi}{\partial \boldsymbol{\sigma}} : \overset{\circ}{\boldsymbol{\sigma}} + \frac{\partial \Phi}{\partial \boldsymbol{\sigma}} \cdot \overset{\circ}{\mathbf{s}} = 0, \tag{2.25}$$

where

$$\overset{\circ}{\mathbf{s}} = (\dot{\bar{\varepsilon}}^p, \dot{f}, \dot{w}_1, \dot{w}_2, \overset{\circ}{\mathbf{n}}{}^{(1)}, \overset{\circ}{\mathbf{n}}{}^{(2)}, \overset{\circ}{\mathbf{n}}{}^{(3)}).$$

More about the theory of the above consistency condition can be found in the paper of Ponte Castañeda and Aravas [2].

Since $\overset{\circ}{\mathbf{n}}{}^{(1)} = \overset{\circ}{\mathbf{n}}{}^{(2)} = \overset{\circ}{\mathbf{n}}{}^{(3)} = \mathbf{0}$, last relation can be rewritten as:

$$\mathbf{N} : \overset{\circ}{\boldsymbol{\sigma}} + \frac{\partial \Phi}{\partial \bar{\varepsilon}^p}\,\dot{\bar{\varepsilon}}^p + \frac{\partial \Phi}{\partial f}\,\dot{f} + \frac{\partial \Phi}{\partial w_1}\,\dot{w}_1 + \frac{\partial \Phi}{\partial w_2}\,\dot{w}_2 = 0.$$

If we substitute $\dot{\bar{\varepsilon}}^p, \dot{w}_1, \dot{w}_2$ from equations (2.15),(2.22),(2.23), we derive:

$$\mathbf{N} : \overset{\circ}{\boldsymbol{\sigma}} - \dot{\lambda}\,H + \frac{\partial \Phi}{\partial f}\dot{f} = 0, \tag{2.26}$$

where

$$H = -\left(\frac{\partial \Phi}{\partial \bar{\varepsilon}^p}\,g_1 + \frac{\partial \Phi}{\partial w_1}\,g_3 + \frac{\partial \Phi}{\partial w_2}\,g_4\right).$$

In case of $H \neq 0$ we have

$$\dot{\lambda} = \frac{1}{H}\left(\mathbf{N} : \overset{\circ}{\boldsymbol{\sigma}} + \frac{\partial \Phi}{\partial f}\,\dot{f}\right). \tag{2.27}$$

It should be noted that the sign of the "hardening modulus" H determines whether the material is hardening of softening:

$$H = \begin{cases} H>0 & \rightarrow \quad \text{hardening,} \\ H<0 & \rightarrow \quad \text{softening.} \end{cases}$$

The terms of hardening or softening can be expressed with the yield surface expanding or contracting respectively. The case where $H = 0$ is called "perfect plasticity" we don't have

either softening either hardening. The concept of perfect plasticity is extensively covered by Lubliner in [19].
If we substitute $\overset{\circ}{\boldsymbol{\sigma}}$ from (2.24) into (2.26):

$$\mathbf{N} : \boldsymbol{\mathcal{L}}^e : \mathbf{D} - \dot{\lambda} \left(\mathbf{N} : \boldsymbol{\mathcal{L}}^e : \mathbf{N} + H \right) + \frac{\partial \Phi}{\partial f} \dot{f}$$

or

$$\dot{\lambda} = \frac{1}{L} \left(\mathbf{N} : \boldsymbol{\mathcal{L}}^e : \mathbf{D} + \frac{\partial \Phi}{\partial f} \dot{f} \right), \tag{2.28}$$

where

$$L = H + \mathbf{N} : \boldsymbol{\mathcal{L}}^e : \mathbf{N}.$$

If we again substitute the expression of $\dot{\lambda}$ from (2.28) into (2.24):

$$\overset{\circ}{\boldsymbol{\sigma}} = \left(\boldsymbol{\mathcal{L}}^e - \frac{1}{L} \boldsymbol{\mathcal{L}}^e : \mathbf{N}\mathbf{N} : \boldsymbol{\mathcal{L}}^e \right) : \mathbf{D} - \frac{1}{L} \frac{\partial \Phi}{\partial f} \boldsymbol{\mathcal{L}}^e : \mathbf{N} \, \dot{f}. \tag{2.29}$$

The Jaumann derivative $\overset{\triangledown}{\boldsymbol{\sigma}}$ is related to $\overset{\circ}{\boldsymbol{\sigma}}$ by the following expression:

$$\overset{\triangledown}{\boldsymbol{\sigma}} = \overset{\circ}{\boldsymbol{\sigma}} + \boldsymbol{\sigma} \cdot \mathbf{W}^p - \mathbf{W}^p \cdot \boldsymbol{\sigma} = \overset{\circ}{\boldsymbol{\sigma}} + \dot{\lambda} \left(\boldsymbol{\sigma} \cdot \boldsymbol{\Omega}^p - \boldsymbol{\Omega}^p \cdot \boldsymbol{\sigma} \right) = \overset{\circ}{\boldsymbol{\sigma}} + \frac{1}{L} (\boldsymbol{\sigma} \cdot \boldsymbol{\Omega}^p - \boldsymbol{\Omega}^p \cdot \boldsymbol{\sigma}) (\mathbf{N} : \boldsymbol{\mathcal{L}}^e : \mathbf{D}). \tag{2.30}$$

Finally, the substitution of $\overset{\circ}{\boldsymbol{\sigma}}$ from (2.29) into (2.30) gives:

$$\overset{\triangledown}{\boldsymbol{\sigma}} = [\boldsymbol{\mathcal{L}}^e - \mathbf{A} (\boldsymbol{\mathcal{L}}^e : \mathbf{N})] : \mathbf{D} - \frac{\partial \Phi}{\partial f} \mathbf{A} \, \dot{f}, \tag{2.31}$$

where

$$\mathbf{A} = \frac{1}{L} (\boldsymbol{\mathcal{L}}^e : \mathbf{N} - \boldsymbol{\sigma} \cdot \boldsymbol{\Omega}^p + \boldsymbol{\Omega}^p \cdot \boldsymbol{\sigma}).$$

The evolution equation of the local porosity can also be written as

$$\dot{f}_{\text{loc}} = \dot{\lambda} \left[(1 - f) N_{kk} + \mathrm{T}(\bar{\varepsilon}^p) g_1 \right] = \frac{1}{L} \left[(1 - f) N_{kk} + \mathrm{T}(\bar{\varepsilon}^p) g_1 \right] \left(\mathbf{N} : \boldsymbol{\mathcal{L}}^e : \mathbf{D} + \frac{\partial \Phi}{\partial f} \dot{f} \right)$$

or

$$\dot{f}_{\text{loc}} = B \left(\mathbf{N} : \boldsymbol{\mathcal{L}}^e : \mathbf{D} + \frac{\partial \Phi}{\partial f} \dot{f} \right), \tag{2.32}$$

where

$$B = \frac{1}{L} \left[(1 - f) N_{kk} + \mathrm{T}(\bar{\varepsilon}^p) g_1 \right].$$

In order to better describe the elastoplastic behavior we can implement the binary plasticity parameter α^p. The expressions for $\mathbf{A}$ and B are modified with respect to the binary plasticity parameter as:

$$\mathbf{A} = \frac{\alpha^p}{L} (\boldsymbol{\mathcal{L}}^e : \mathbf{N} - \boldsymbol{\sigma} \cdot \boldsymbol{\Omega}^p + \boldsymbol{\Omega}^p \cdot \boldsymbol{\sigma})$$

and

$$B = \frac{\alpha^p}{L} \left[(1 - f) N_{kk} + \mathrm{T}(\bar{\varepsilon}^p) \, g_1 \right].$$

If $\alpha^p = 1$, then elastoplastic behaviour occurs and the equations describing the behaviour of the material are (2.31), (2.32). When the behavior is elastic, $\alpha^p = 0$.

Chapter 3

Numerical implementation

3.1 Non - local implementation

As we previously mentioned, non-local constitutive models cannot be handled by the commercial finite element codes, that are commonly used for the solution of structural mechanics problems. Here, we take advantage of the similarities between the BVP that defines the non-local variable f and the steady-state heat transfer problem in an isotropic material, and use the available elements in commercial codes for coupled thermo-mechanical analysis of structures (Seupel et al. [27], Papadioti et al. [22]).
One version of the steady-state heat transfer problem in an isotropic material is

$$k\,\nabla^2 T + r\,(\Delta\boldsymbol{\varepsilon}, T) = 0 \quad \text{in} \quad \Omega \tag{3.1}$$

$$k\,\mathbf{n}\cdot\nabla T = \hat{q} \quad \text{on} \quad \partial\Omega, \tag{3.2}$$

where T is temperature, k the thermal conductivity, r the heat supply per unit volume, $\hat{q}$ the prescribed boundary flux vector, and $\Delta\varepsilon$ a strain increment properly defined in terms of nodal displacements.
As we previously mentioned in Chapter 2 the BVP problem for the non-local porosity is :

$$\ell^2\,\nabla^2 f - f + f_{\text{loc}}(\Delta\boldsymbol{\varepsilon}, f) = 0 \quad \text{in} \quad \Omega \tag{3.3}$$

$$\frac{\partial f}{\partial n} \equiv \mathbf{n}\cdot\nabla f = 0 \quad \text{on} \quad \partial\Omega. \tag{3.4}$$

Comparing the BVP (3.1)–(3.2) and (3.3)–(3.4), we conclude that the non-local variable f can be identified with the temperature field T provided the following correspondence is used (Papadioti et al. [22]):

$$T \leftrightarrow f, \tag{3.5}$$

$$\kappa \leftrightarrow \ell^2, \tag{3.6}$$

$$r\,(\Delta\boldsymbol{\varepsilon}, T) \leftrightarrow f_{loc}\,(\Delta\boldsymbol{\varepsilon}, f) - f, \tag{3.7}$$

$$\hat{q} \leftrightarrow 0. \tag{3.8}$$

So in the special case of quasi-static problems, the solution can be also obtained using user material subroutine UMAT in ABAQUS/STANDARD together with a *COUPLED

TEMPERATURE-DISPLACEMENT, STADY STATE analysis option.
The constitutive equations are integrated numerically in user subroutine UMAT. In UMAT the value of the non local porosity f is provided as "temperature", f_{loc} is determined from the numerical integration of the constitutive equation using the algorithm presented in section 3.2 and r (variable RPL IN UMAT) is identified with the difference $f_{\text{loc}} - f$. The derivatives $\frac{\partial \Delta \boldsymbol{\sigma}}{\partial \Delta \boldsymbol{\varepsilon}}$, $\frac{\partial \boldsymbol{\sigma}}{\partial T}$, $\frac{\partial r}{\partial \Delta \boldsymbol{\varepsilon}}$, $\frac{\partial r}{\partial T}$ are also evaluated in UMAT.
It should be also noted that the coupled temperature - displacement in ABAQUS/Standard can be used for the solution of quasi-static implicit strain-gradient plasticity problems, but it cannot be used for dynamic problems, in which inertia effects become important.

3.2 Numerical Integration of the Constitutive Equations

In this section, the numerical integration of the constitutive equations is described. In a finite element environment, the solution is developed incrementally and the constitutive equations are integrated numerically at the element Gauss integration points. Let $\mathbf{F}$ denote the deformation gradient tensor. At a given Gauss point, the solution $(\mathbf{F}_n, \boldsymbol{\sigma}_n, \mathbf{s}_n)$ at time t_n as well as the deformation gradient $\mathbf{F}_{n+1}$ at time $t_{n+1} = t_n + \Delta t$ are known and the problem is to determine $(\boldsymbol{\sigma}_{n+1}, \mathbf{s}_{n+1})$.

The time variation of the deformation gradient $\mathbf{F}$ can be written as:

$$\mathbf{F}(t) = \Delta\mathbf{F}(t) \cdot \mathbf{F}_n = \mathbf{R}(t) \cdot \mathbf{U}(t) \cdot \mathbf{F}_n, \quad t \in [t_n, t_{n+1}], \tag{3.9}$$

where $\mathbf{R}(t)$ and $\mathbf{U}(t)$ are the relative rotation and the relative right stretch tensors associated with $\Delta\mathbf{F}(t)$. The corresponding deformation rate $\mathbf{D}(t)$ and spin $\mathbf{W}(t)$ tensors are given by

$$\mathbf{D}(t) = [\dot{\mathbf{F}}(t) \cdot \mathbf{F}^{-1}(t)]^{(\text{sym})} = [\Delta\dot{\mathbf{F}}(t) \cdot \Delta\mathbf{F}^{-1}(t)]^{(\text{sym})} \tag{3.10}$$

and

$$\mathbf{W}(t) = [\dot{\mathbf{F}}(t) \cdot \mathbf{F}^{-1}(t)]^{(\text{skew})} = [\Delta\dot{\mathbf{F}}(t) \cdot \Delta\mathbf{F}^{-1}(t)]^{(\text{skew})}. \tag{3.11}$$

The aforementioned relative rotation tensor $\mathbf{R}(t)$ is used to define the so-called "rotation-neutralized quantities" $\hat{\boldsymbol{\sigma}}(t)$ and $\hat{\mathbf{n}}^{(i)}$:

$$\hat{\boldsymbol{\sigma}}(t) = \mathbf{R}^T(t) \cdot \boldsymbol{\sigma}(t) \cdot \mathbf{R}(t), \tag{3.12}$$

$$\hat{\mathbf{n}}^{(i)}(t) = \mathbf{R}^T(t) \cdot \mathbf{n}(t), \tag{3.13}$$

If it is assumed that the Lagrangian triad associated with $\Delta\mathbf{F}(t)$ remains fixed in the time interval $[t_n, t_{n+1}]$, it can be shown readily that

$$\mathbf{D} = \mathbf{R} \cdot \dot{\mathbf{E}} \cdot \mathbf{R}^T, \qquad \mathbf{W} = \dot{\mathbf{R}} \cdot \mathbf{R}^T, \tag{3.14}$$

$$\overset{\triangledown}{\boldsymbol{\sigma}} = \mathbf{R} \cdot \dot{\hat{\boldsymbol{\sigma}}} \cdot \mathbf{R}^T, \qquad \overset{\triangledown}{\mathbf{n}}^{(i)} = \mathbf{R} \cdot \dot{\hat{\mathbf{n}}}^{(i)}, \tag{3.15}$$

where $\mathbf{E}(t) = \ln \mathbf{U}(t)$ is the logarithmic strain relative to the configuration at t_n.
Taking into account the $\Phi, \mathbf{N}, g_1, g_2, g_3, g_4$ and $\boldsymbol{\Omega}^{\mathbf{p}}$ are isotropic functions of their arguments,

the elastoplastic equations can be written in the form:

$$\dot{\mathbf{E}} = \dot{\mathbf{E}}^e + \dot{\mathbf{E}}^p, \tag{3.16}$$

$$\Phi(\hat{\boldsymbol{\sigma}}, \hat{\mathbf{s}}) = 0, \tag{3.17}$$

$$\dot{\mathbf{E}}^p = \dot{\lambda}\, \mathbf{N}(\hat{\boldsymbol{\sigma}}, \hat{\mathbf{s}}), \tag{3.18}$$

$$\dot{\bar{\varepsilon}}^p = \dot{\lambda}\, g_1(\hat{\boldsymbol{\sigma}}, \hat{\mathbf{s}}) = \frac{\hat{\boldsymbol{\sigma}} : \dot{\mathbf{E}}^p}{(1-f)\sigma_y(\bar{\varepsilon}^p)}, \tag{3.19}$$

$$\dot{f}_{\text{loc}} = \dot{\lambda}\, [(1-f)N_{kk} + \mathrm{T}(\bar{\varepsilon}^p) g_1(\hat{\boldsymbol{\sigma}}, \hat{\mathbf{s}})] = (1-f)\dot{E}^p_{kk} + \mathrm{T}(\bar{\varepsilon}^p)\dot{\bar{\varepsilon}}^p, \tag{3.20}$$

$$\dot{\hat{\boldsymbol{\sigma}}} = \hat{\boldsymbol{\mathcal{L}}}^e : \dot{\mathbf{E}}^e + \dot{\lambda}[\hat{\boldsymbol{\sigma}} \cdot \boldsymbol{\Omega}^p(\hat{\boldsymbol{\sigma}}, \hat{\mathbf{s}}) - \boldsymbol{\Omega}^p(\hat{\boldsymbol{\sigma}}, \hat{\mathbf{s}}) \cdot \hat{\boldsymbol{\sigma}}], \tag{3.21}$$

$$\dot{w}_1 = \dot{\lambda}\, g_2(\hat{\boldsymbol{\sigma}}, \hat{\mathbf{s}}) = \left(\hat{\mathbf{n}}^{(3)}\hat{\mathbf{n}}^{(3)} - \hat{\mathbf{n}}^{(1)}\hat{\mathbf{n}}^{(1)}\right) : \hat{\boldsymbol{\mathcal{A}}} : \dot{\mathbf{E}}^p, \tag{3.22}$$

$$\dot{w}_2 = \dot{\lambda}\, g_3(\hat{\boldsymbol{\sigma}}, \hat{\mathbf{s}}) = \left(\hat{\mathbf{n}}^{(3)}\hat{\mathbf{n}}^{(3)} - \hat{\mathbf{n}}^{(2)}\hat{\mathbf{n}}^{(2)}\right) : \hat{\boldsymbol{\mathcal{A}}} : \dot{\mathbf{E}}^p, \tag{3.23}$$

where

$$\hat{\mathcal{A}}_{ijpq} = R^T_{ik}\, R^T_{jl}\, R^T_{pm}\, R^T_{qn}\, \mathcal{A}_{klmn},$$
$$\hat{\mathcal{C}}_{ijpq} = R^T_{ik}\, R^T_{jl}\, R^T_{pm}\, R^T_{qn}\, \mathcal{C}_{klmn},$$
$$\hat{\mathcal{L}}^e_{ijpq} = R^T_{ik}\, R^T_{jl}\, R^T_{pm}\, R^T_{qn}\, \mathcal{L}^e_{klmn},$$

and

$$\hat{\mathbf{s}} = \{\bar{\varepsilon}^p, f, w_1, w_2, \hat{\mathbf{n}}^{(1)}, \hat{\mathbf{n}}^{(2)}, \hat{\mathbf{n}}^{(3)}\}.$$

After stating the rotation neutralized equations, we now will present their integration algorithm. Equation (3.16) is integrated exactly:

$$\Delta\dot{\mathbf{E}} = \Delta\dot{\mathbf{E}}^e + \Delta\mathbf{E}^p \quad \Rightarrow \quad \Delta\dot{\mathbf{E}}^e = \Delta\dot{\mathbf{E}} - \Delta\dot{\mathbf{E}}^p.$$

We are using the backward euler scheme for the following equations:

$$\Delta\dot{\mathbf{E}}^p = \Delta\lambda\, \mathbf{N}_{n+1}, \quad \mathbf{N}_{n+1} = \mathbf{N}\left(\hat{\boldsymbol{\sigma}}_{n+1}, f, w_\alpha|_{n+1}, \hat{\mathbf{n}}^{(i)}_{n+1}\right), \tag{3.24}$$

$$\Delta\bar{\varepsilon}^p = \frac{\hat{\boldsymbol{\sigma}}_{n+1} : \Delta\mathbf{E}^p}{(1-f)\sigma_y(\bar{\varepsilon}^p_{n+1})} \equiv \mathbf{R}_2 : \Delta\mathbf{E}^p, \tag{3.25}$$

$$\Delta f_{\text{loc}} = (1-f)\Delta E^p_{kk} + \mathrm{T}(\bar{\varepsilon}^p_{n+1}). \tag{3.26}$$

Finally, a forward euler method is used for the numerical integration of the elasticity equation (3.21) and the evolution equations (3.22)-(3.23) of the aspect ratios:

$$\begin{aligned}\hat{\boldsymbol{\sigma}}_{n+1} &= \boldsymbol{\sigma}_n + \boldsymbol{\mathcal{L}}^e_n : \Delta\mathbf{E} - \boldsymbol{\mathcal{L}}^e_n : \Delta\mathbf{E}^p + \Delta\lambda(\boldsymbol{\sigma}_n \cdot \boldsymbol{\Omega}^p_n - \boldsymbol{\Omega}^p_n \cdot \boldsymbol{\sigma}_n) = \\ &\equiv \boldsymbol{\sigma}^e + \boldsymbol{\sigma}^{pc} + \Delta\lambda\, \mathbf{R}_1,\end{aligned} \tag{3.27}$$

$$\Delta w_\alpha = w_\alpha|_n \left(\mathbf{n}^{(3)}_n \mathbf{n}^{(3)}_n - \mathbf{n}^{(\alpha)}_n \mathbf{n}^{(\alpha)}_n\right) : \mathcal{A}_n : \Delta\mathbf{E}^p \equiv \mathbf{R}_{3\alpha} : \Delta\mathbf{E}^p, \tag{3.28}$$

where $\boldsymbol{\sigma}^e = \boldsymbol{\sigma}_n + \boldsymbol{\mathcal{L}}^e_n : \Delta\mathbf{E}$ is the "elastic predictor" and $\boldsymbol{\sigma}^{pc} = -\boldsymbol{\mathcal{L}}^e_n : \Delta\mathbf{E}^p$ the "plastic corrector".
The quantities of $\Delta\lambda$ and $\Delta\mathbf{E}^p$ are chosen as the primary unknowns and the yield condition and the plastic flow rule

$$\Phi(\Delta\lambda, \Delta\mathbf{E}^p) = 0, \tag{3.29}$$

$$\Delta\mathbf{E}^p - \Delta\lambda\, \mathbf{N}(\Delta\lambda, \Delta\mathbf{E}^p) = \mathbf{0}, \tag{3.30}$$

are treated as the basic equations. The Newton-Raphson method will be used to solve the system. In every Newton iteration, for the current values of $\Delta\lambda$ and $\Delta\mathbf{E}^p$, $\hat{\boldsymbol{\sigma}}_{n+1}$ is calculated by using (3.27), $(w_\alpha|_{n+1}, \hat{\mathbf{n}}^{(i)}_{n+1})$ are determined from (3.28), and $(\Delta\bar{\varepsilon}^p, \Delta f)$ are calculated by solving numerically the system of non-linear equations (3.25) and (3.26) with Newton's method.

Finally, we compute:

$$\boldsymbol{\sigma}_{n+1} = \mathbf{R}_{n+1} \cdot \boldsymbol{\sigma}_{n+1} \cdot \mathbf{R}^T_{n+1} \tag{3.31}$$

and

$$\mathbf{n}^{(i)}_{n+1} = \mathbf{R}_{n+1} \cdot \hat{\mathbf{n}}^{(i)}_{n+1}. \tag{3.32}$$

3.3 Linearization moduli

When using the finite element method, we also need to calculate the linearization moduli. In particular we need to calculate the following derivatives $\frac{\partial\Delta\boldsymbol{\sigma}}{\partial\Delta\boldsymbol{\varepsilon}}$, $\frac{\partial\boldsymbol{\sigma}}{\partial T} = \frac{\partial\boldsymbol{\sigma}}{\partial f}$, $\frac{\partial r}{\partial\Delta\boldsymbol{\varepsilon}} = \frac{\partial f_{\rm loc}}{\partial\Delta\boldsymbol{\varepsilon}}$, $\frac{\partial r}{\partial T} = \frac{\partial f_{\rm loc}}{\partial f} - 1$. From equation (2.31) we derive

$$\frac{\partial\Delta\boldsymbol{\sigma}}{\partial\Delta\boldsymbol{\varepsilon}} \simeq \boldsymbol{\mathcal{L}}^e - \mathbf{A}(\boldsymbol{\mathcal{L}}^e : \mathbf{N}), \qquad \mathbf{A} = \frac{1}{L}\left(\boldsymbol{\mathcal{L}}^e : \mathbf{N} - \boldsymbol{\sigma}\cdot\boldsymbol{\Omega}^p + \boldsymbol{\Omega}^p\cdot\boldsymbol{\sigma}\right), \tag{3.33}$$

$$\frac{\partial\boldsymbol{\sigma}}{\partial f} \simeq -\frac{\partial\Phi}{\partial f}\mathbf{A}. \tag{3.34}$$

From equation (2.32) we have

$$\frac{\partial f_{\rm loc}}{\partial\Delta\boldsymbol{\varepsilon}} \simeq B\,\mathbf{N} : \boldsymbol{\mathcal{L}}^e, \qquad B = \frac{1}{L}\left[(1-f)N_{kk} + \mathrm{T}(\bar{\varepsilon}^p)\,g_1\right], \tag{3.35}$$

$$\frac{\partial f_{\rm loc}}{\partial f} \simeq B\,\frac{\partial\Phi}{\partial f}. \tag{3.36}$$

3.4 The role of UMAT

The constitutive model described above is implemented into the ABAQUS general purpose finite element code [1]. Non-local constitutive models cannot be handled by the commercial finite element codes, that are commonly used for the solution of structural mechanics problems. Here, we take advantage of the similarities between the BVP that defines the non-local variable f and the steady-state heat transfer problem in an isotropic material, and use the available elements in commercial codes for coupled thermo-mechanical analysis of structures (Seupel et al. [27], Papadioti et al. [22]).

ABAQUS provides a general interface so that a particular constitutive model can be introduced via a "user subroutine" named UMAT (UserMATerial). UMAT can be used in special cases that the material is not an ABAQUS Standard Material and the mechanical constitutive behavior of a material needs to be defined.

The subroutine contains solution-dependent state variables (STATEV) that are defined by

the user. Below we present some predefined variables in UMAT.

DDSDDE(NTENS,NTENS) As the name states this variable is the Jacobian matrix of the material defined as $\frac{\partial \Delta \boldsymbol{\sigma}}{\partial \Delta \boldsymbol{\varepsilon}}$, where $\boldsymbol{\sigma}$ is the stress applied and $\boldsymbol{\varepsilon}$ is the strain. The Jacobian will be calculated for every increment, starting from 1 and finishing with NTENS. Where NTENS is the Number of total stress components. This action will be performed in all the dimensions of the problem. For instance, in a 2D problem, we will end up with a matrix $(4, 4)$. Unless you invoke the unsymmetric equation solution capability for the user-defined material, Abaqus/Standard will use only the symmetric part of DDSDDE.

STRESS(NTENS) Which is an array containing the stress components of the material. The size of this array depends on the value of NTENS as defined below. In finite-strain problems the stress tensor has already been rotated to account for rigid body motion in the increment before UMAT is called, so that only the corotational part of the stress integration should be done in UMAT. The measure of stress used is "true" (Cauchy) stress.

NSTATEV The number of extra state variables to be used

STATEV(NSTATV) An array containing the solution-dependent state variables. These are passed in as the values at the beginning of the increment unless they are updated in user subroutines USDFLD or UEXPAN, in which case the updated values are passed in. In all cases STATEV must be returned with the updated values at the end of the increment.

Other variables that are also be defined are:
NDI Number of direct stress components
NSHR Number of shear stress components
NPROPS Number of material constants
NOEL Number of Element being processed
NPT Number of Integration point being processed
LAYER Layer number (for composite shells and solids)
KSPT Section point number within the current layer
KINC Increment number
KSTEP Step number
PROPS(NPROPS) Array containing the user specifined material constants
STRAN(NTENS) Array containing the total strains
DSTRAN(NTENS) Array containing the strain increments
TIME(1) Step time at the beginning of the current increment
TIME(2) Total time at the beginning of the current increment
DTIME Time increment
PNEWDT Ratio DTIMEnew=DTIMEcurrent
DROT(3,3) Rotation increment matrix
DFGRD0(3,3) Deformation gradient at the start of the increment

DFGRD1(3,3) Deformation gradient at the end of the increment
CMNAME User-Defined material name

All the solution dependent variables and stresses are updated at the end of every increment.

Chapter 4

Applications

4.1 Unit Cell theory

In porous materials, tiny pores are scattered throughout the body. Here we consider three-dimensional cubic unit cells with one pore at the center. Our goal is to compare the results of our constitutive model for porous metals with the results of the unit cell calculations. All calculations are carried out using the ABAQUS general purpose finite element code. Specifically, we gather all the material's pores volume and create a pore with the total volume of all the smaller pores added. Then we place this pore at the center of the unit cell and simulate the new geometry. In the following we present the steps needed to create such a geometry. The von Mises plasticity model is used for the matrix material in the finite element unit cell calculations.

4.1.1 NETGEN and model discretization

The first step is to create the geometry and the discretization that will later be imported in Abaqus to run the simulations. The program used for the creation of the geometry file is NETGEN/NGSolve.

Creating the NETGEN input file: With the command solid $sph1 = sphere(0.5, 0.5, 0.5; 0.1)$ we create a solid sphere with a radius of 0.1 in the length unit chosen.
At this point we should note that 1% porosity is not directly connected to the radius of the centered solid sphere. For instance,

$$\text{porosity} = f \quad \Leftrightarrow \quad \frac{V_{\text{voids}}}{V_{\text{total}}} = f \quad \Leftrightarrow \quad \frac{\frac{4}{3}\,\pi\,R^3}{L^3} = f \quad \Leftrightarrow \quad R = L\left(\frac{3\,f}{4\,\pi}\right)^{1/3},$$

where $L = 1$ is the size of the unit cubic cell. The same concept will be used for all the porosity values used in our calculations.
After creating the centered sphere, we end up with the geometry shown in Figure 4.1.
The second step is the finite element discretization. Three-dimensional 10-node quadratic tetrahedral elements are used. Figure 4.2 illustrates a finite element mesh with 190.045 degrees of freedom. Mesh sensitivity studies reveal that meshes with more than 180.000

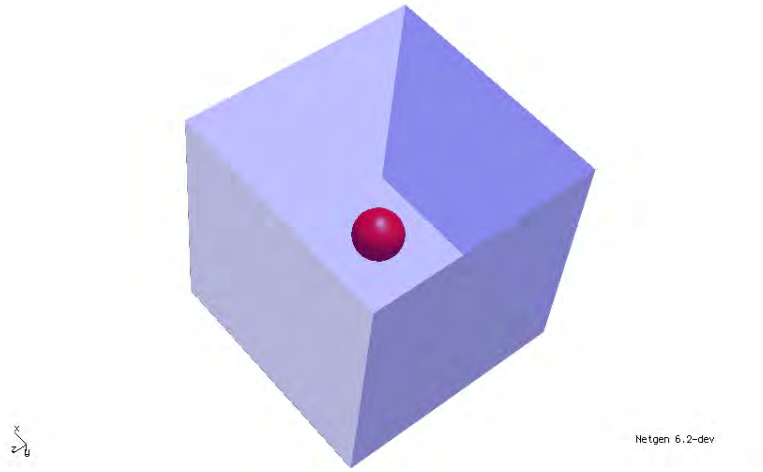

Figure 4.1: Geometry created with NETGEN for initial porosity $f_0 = 0.01$

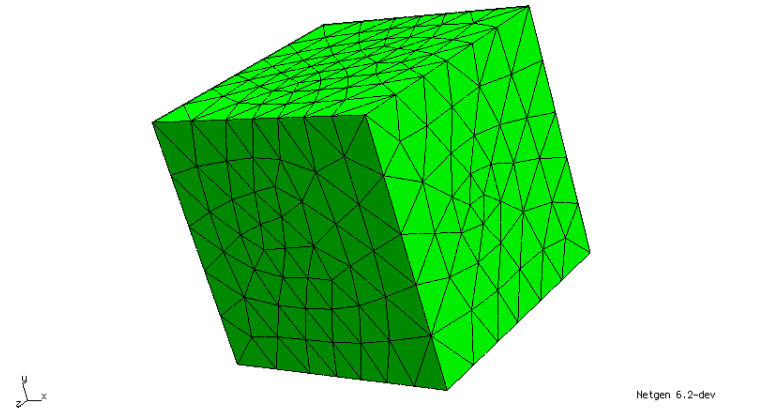

Figure 4.2: Finite element discretization of the cubic unit cell

degrees of freedom produce accurate results [21]. The third and final step is to export the mesh to an ABAQUS file format. NETGEN creates one file with the nodes and the elements and another one with the constraints that ensure the periodicity of the mesh.
In our calculations C3D10H elements are used. The reason for using the "hybrid" elements is that the matrix material response is incompressible. Hybrid elements use an independent interpolation for the hydrostatic stress. In the calculations, we use a nearly incompressible matrix material, in which the elastic bulk modulus is much larger than the elastic shear modulus.

4.1.2 The role of UHARD subroutine

The von Mises plasticity model is used in the finite element calculations. To define the elastoplastic behavior of the material we use the ABAQUS "user subroutine" UHARD.

UHARD is called at all integration points of the model, where user-defined isotropic functions are used and provides the material behavior. In UHARD we need to define the variables SYIELD, HARD(1), HARD(2) and HARD(3):

SYIELD: yield stress σ_y for isotropic plasticity,

HARD(1): variation of SYIELD expressed with respect to the equivalent plastic strain $\bar{\varepsilon}^p$, i.e., $\partial\sigma_y/\partial\bar{\varepsilon}^p$.

In our applications the flow stress of the matrix material σ_y is a function of the corresponding equivalent plastic strain $\bar{\varepsilon}^p$:

$$\sigma_y(\bar{\varepsilon}^p) = \sigma_0 \left(1 + \frac{\bar{\varepsilon}^p}{\varepsilon_0}\right)^{1/n}, \quad \text{so that} \quad \frac{d\sigma_y}{d\bar{\varepsilon}^p} = \frac{\sigma_0}{n}\left(1 + \frac{\bar{\varepsilon}^p}{\varepsilon_0}\right)^{(1/n)-1} \frac{1}{\varepsilon_0} = \frac{\sigma_y}{n(\varepsilon_0 + \bar{\varepsilon}^p)}, \tag{4.1}$$

where σ_0 is the yield stress of the matrix material, $\varepsilon_0 = \sigma_0/E$, E is the elastic Young's modulus, and n the hardening exponent, which takes values in the range $1 \leq n \leq \infty$. The limiting case $n = \infty$ corresponds to perfect plasticity. The values $E = 300\,\sigma_0$, $\nu = 0.3$, and $n = 10$ are used in the calculations.

4.2 Uniaxial tension

4.2.1 Introduction

First, we are going to study the problem of uniaxial tension. Before proceeding with the results we should note that the same calculations are conducted with two versions of the anisotropic costitutive model for porous metals. The first version is the original variational method and the second is the modified variational method proposed by Danas [7]. The purpose of the modification was to improve the predictions of the constitutive model under high triaxiality loading conditions. The main idea is that by examining multiple loading cases and initial porosities f_0 we will be able to conclude how effective this modification is. We are going to present the stress-strain curve as well as the evolution of the porosity and the aspect ratio as the material deforms plastically.

We note that the equivalent plastic strain is defined as

$$\bar{\varepsilon}^p = \int_0^t \sqrt{\frac{2}{3}\, D^p_{ij}\, D^p_{ij}}\; dt,$$

where t is a time-like (loading) parameter. The values labeled "ebar" in the plots that follow are *average values* of $\bar{\varepsilon}^p$ in the matrix.

The "triaxiality" XS is the ratio of the hydrostatic stress to the von Mises equivalent stress:

$$XS = \frac{p}{\sigma_e}, \qquad p = \frac{\sigma_{kk}}{3}, \qquad \sigma_e = \sqrt{\frac{3}{2}\,\sigma^{\rm dev}_{ij}\,\sigma^{\rm dev}_{ij}}, \tag{4.2}$$

where $\sigma_{ij}^{\text{dev}} = \sigma_{ij} - p\,\delta_{ij}$ are the components of the stress deviator. **Note** that in the graphs shown bellow the stress axis represents the value of stress divided with the value of σ_0.

In the following graphs the label UMAT-mvar denotes the results of the modified version of the model according to Danas and Aravas [7] and the UMAT-var indicates the results of the original variational method. For the case of uniaxial tension we carried out calculations with initial porosity $f_0 = 1\%,\ 2\%$ and 3%. In the case of the triaxiality control we studied the following cases:

- initial porosity $f_0 = 1\%$ and triaxialities $XS = 1, XS = 2, XS = 3$,
- initial porosity $f_0 = 2\%$ and triaxialities $XS = 1, XS = 2, XS = 3$,
- initial porosity $f_0 = 3\%$ and triaxialities $XS = 1, XS = 2, XS = 3$,
- initial porosity $f_0 = 5\%$ and triaxialities $XS = 1, XS = 2, XS = 3$.

In the following, we present the most representative cases.

4.2.2 Porosity 1%

We start with the problem of uniaxial tension ($XS = 1/3$) with initial porosity $f_0 = 1\%$. As we can see from the graphs below, regarding the stress-strain curves both versions of the constitutive model agree with the unit cell calculations. However, the modified variational method seems to overestimate the evolution of the porosity, whereas the original variational method agrees very well with the unit cell calculations. As far as the equivalent plastic strain is concerned, there seems to be a perfect match between the two versions of the constitutive model and the unit cell calculations. Regarding the aspect ratio, there is a general good agrement between the results, but the original model seems to perform better.

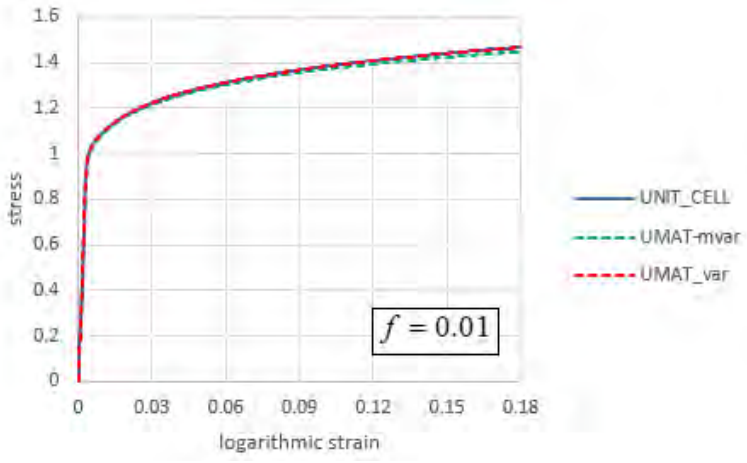

Figure 4.3: Stress-Strain curves in uniaxial tension for initial porosity $f_0 = 1\%$

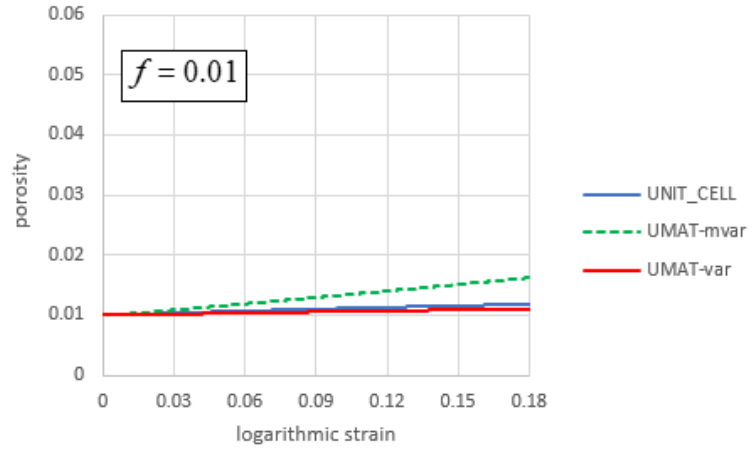

Figure 4.4: Porosity evolution curves in uniaxial tension for initial porosity $f_0 = 1\%$

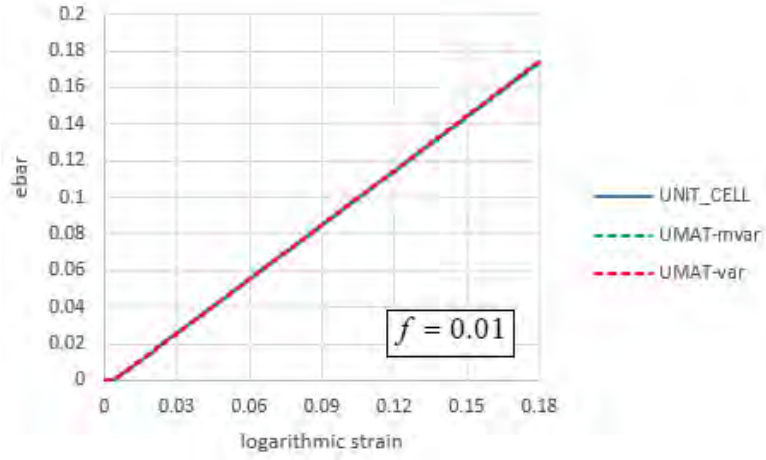

Figure 4.5: Evolution of equivalent plastic strain in the matrix for in uniaxial tension and initial porosity $f_0 = 1\%$

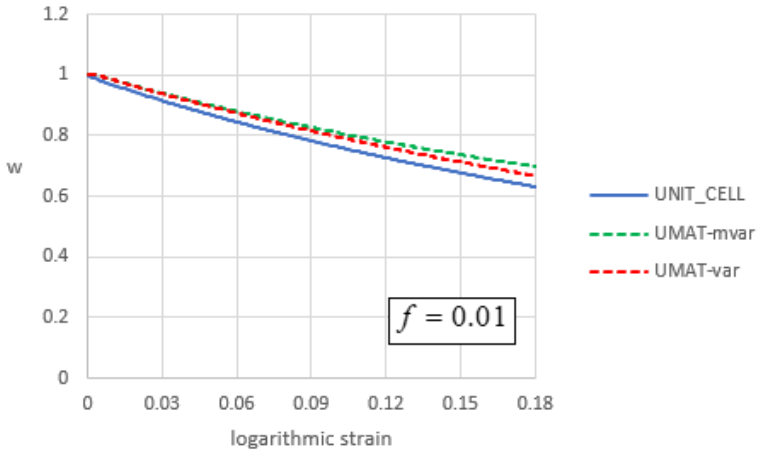

Figure 4.6: Aspect ratio evolution curves in uniaxial tension for initial porosity $f_0 = 1\%$

4.2.3 Porosity 3%

We continue with the problem of uniaxial tension ($XS = 1/3$) and an initial porosity $f_0 = 3\%$. As we can see from the graphs below, regarding the stress-strain curves both versions of the constitutive model agree with the unit cell calculations. However, the modified variational method once again seems to overestimate the evolution of the porosity but not to the same extent as in the case of $f_0 = 1\%$. As far as the equivalent plastic strain is concerned, there seems to be a perfect match between the two versions of the constitutive model and the unit cell calculations. Regarding the aspect ratio there is a general good agrement between the results, and seems to be a better agrement compared to 1 % initial porosity.

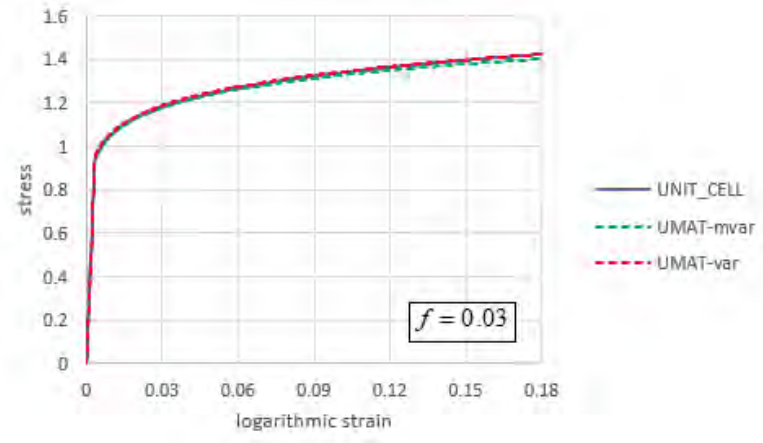

Figure 4.7: Stress-Strain curves in uniaxial tension for initial porosity $f_0 = 3\%$

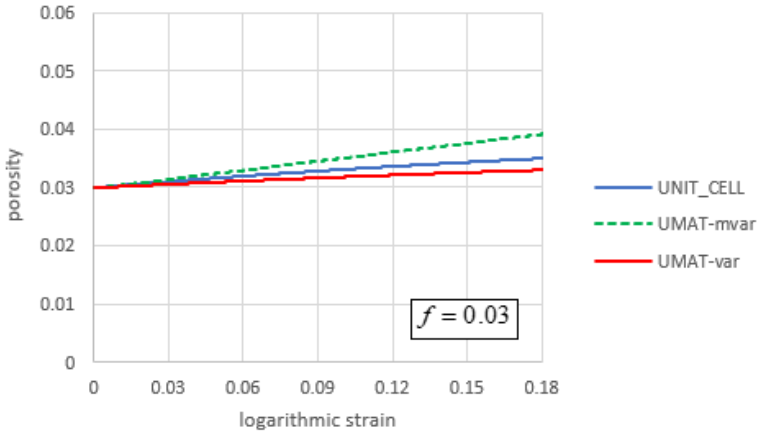

Figure 4.8: Porosity evolution curves in uniaxial tension for initial porosity $f_0 = 3\%$

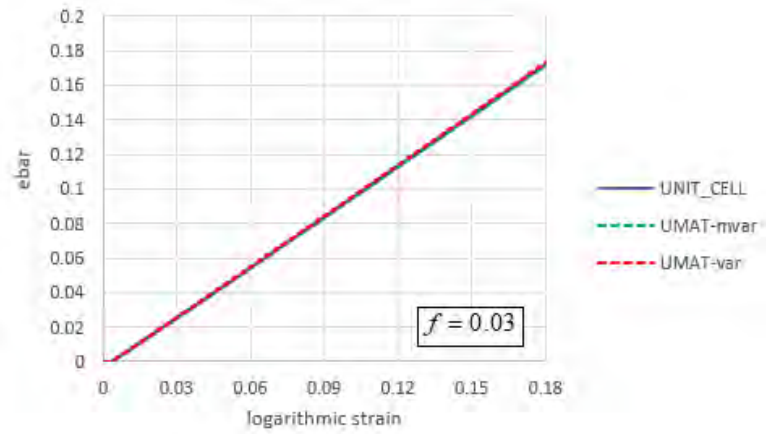

Figure 4.9: Ebar evolution curves in uniaxial tension for initial porosity $f_0 = 3\%$

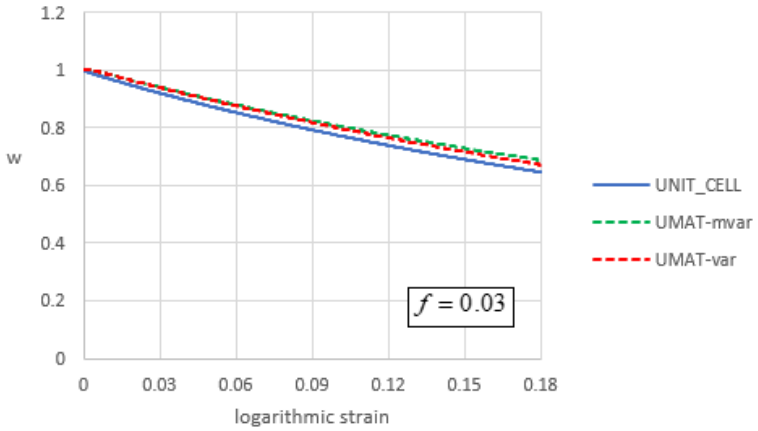

Figure 4.10: Aspect ratio evolution curves in uniaxial tension for initial porosity $f_0 = 3\%$

4.3 Triaxiality control

Here we are going to study the problem of tension under different triaxiality loading conditions (uniaxial tension plus hydrostatic stress). The values of triaxiality $XS = 1$ and 3 and initial porosities $f_0 = 1\%$ and 5% are used to test the performance of the modified variational method.

4.3.1 $f_0 = 1\%$ initial porosity and Triaxiality $XS = 1$

We start with the case of initial porosity $f_0 = 1\%$ and triaxiality equal to 1. As we can see from the graphs below, regarding the stress-strain curves there seems to be a mismatch between the results of the modified variational method and the other two methods. The porosity graph shows that neither the modified variational method nor the original model agrees well with the unit cell calculations. The modified version of the model seems once again to overestimate the porosity but this time more aggressively whereas the original model underestimates the evolution of porosity. As far as the equivalent plastic strain is concerned,

there seems to be a perfect match between the two versions of the constitutive model and the unit cell calculations. The aspect ratio seems to be predicted more accurately by the modified model.

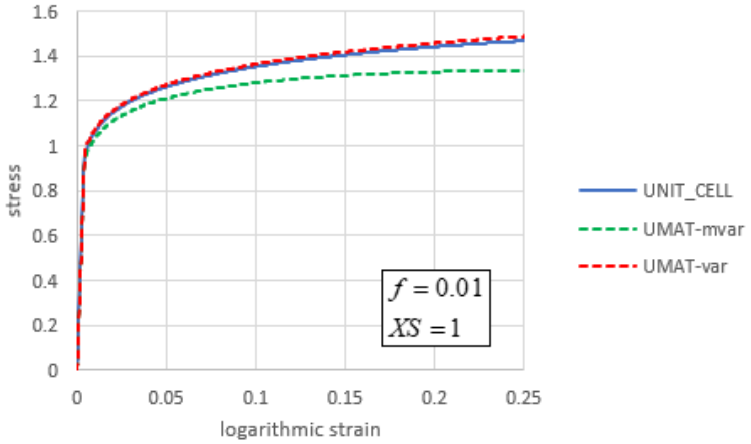

Figure 4.11: Stress-Strain curves in tension for initial porosity $f_0 = 1\%$ and triaxiality $XS = 1$

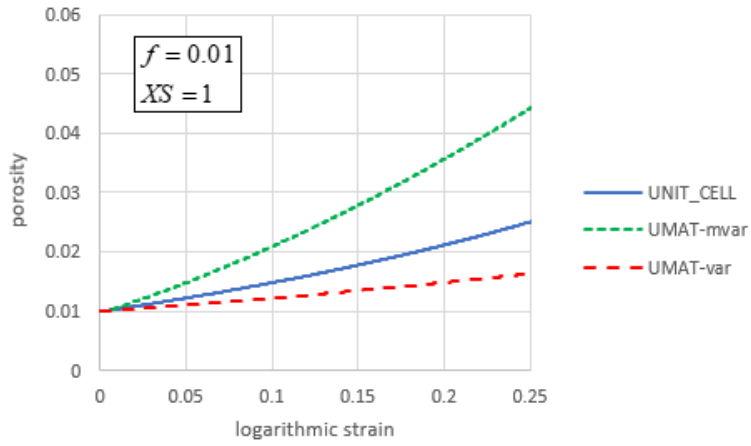

Figure 4.12: Porosity evolution curves in tension for initial porosity $f_0 = 1\%$ and triaxiality $XS = 1$

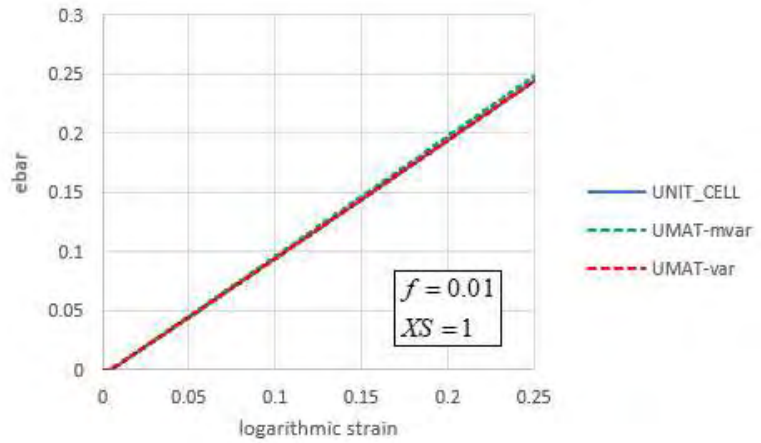

Figure 4.13: Evolution of equivalent plastic strain in tension for initial porosity $f_0 = 1\%$ and triaxiality $XS = 1$

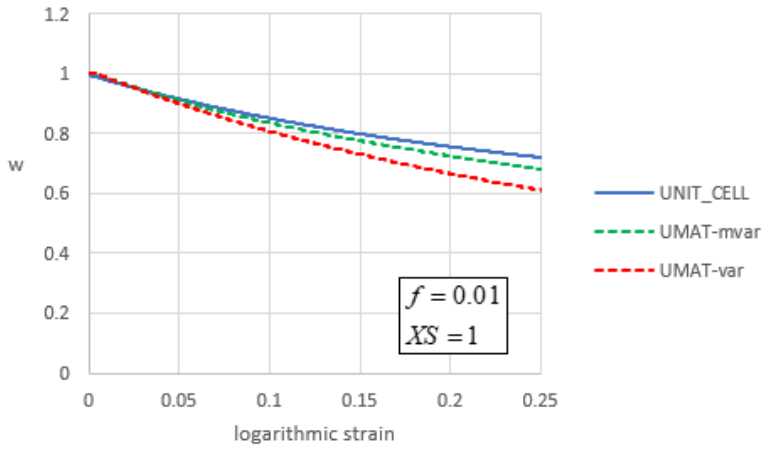

Figure 4.14: Aspect Ratio evolution curves in tension for initial porosity $f_0 = 1\%$ and triaxiality $XS = 1$

4.3.2 $f_0 = 1\%$ initial porosity and Triaxiality $XS = 3$

We continue with the case of initial porosity $f_0 = 1\%$ and triaxiality equal to 3. Figure 4.15 shows contour plots of the von Mises equivalent stress at a macroscopic logarithmic strain of 10%. We were not able to apply larger strains due to the excessive element distortion. As we can see from the graphs below, the modified variational method predicts more accurately the stress-strain curves, the porosity evolution, and the aspect ratio. As far as the equivalent plastic strain is concerned, there seems to be a perfect match between the two versions of the constitutive model and the unit cell calculations.

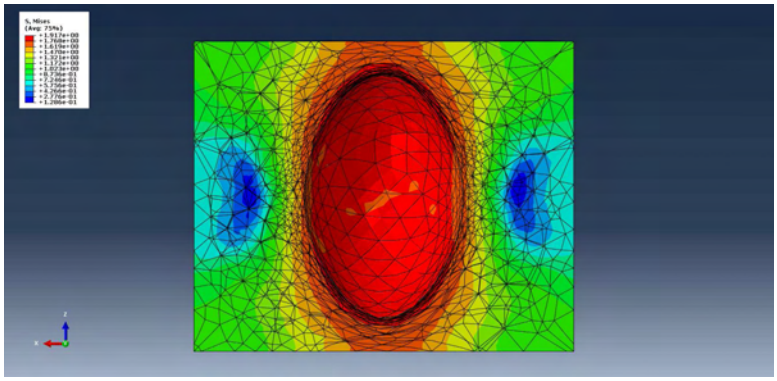

Figure 4.15: Contour plots of the mises stress for initial porosity $f = 1\%$ and $XS = 3$

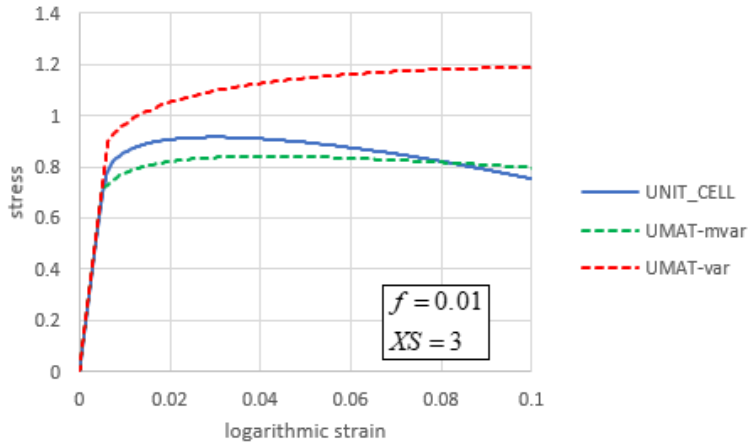

Figure 4.16: Stress-Strain curves in tension for initial porosity $f_0 = 1\%$ and triaxiality $XS = 3$

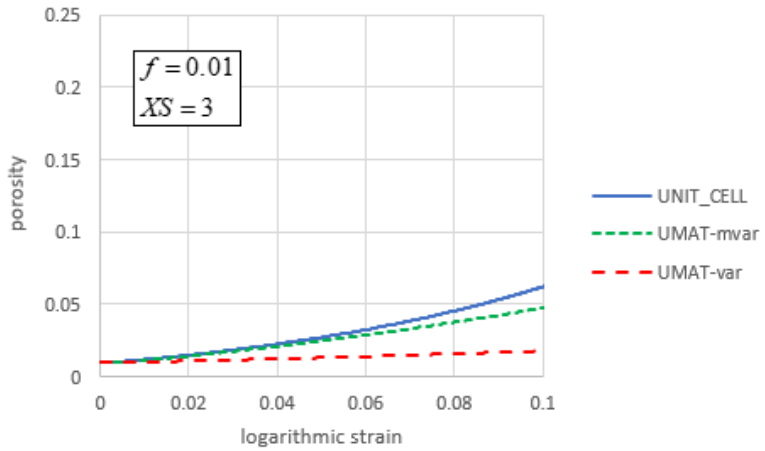

Figure 4.17: Porosity evolution curves in tension for initial porosity $f_0 = 1\%$ and triaxiality $XS = 3$

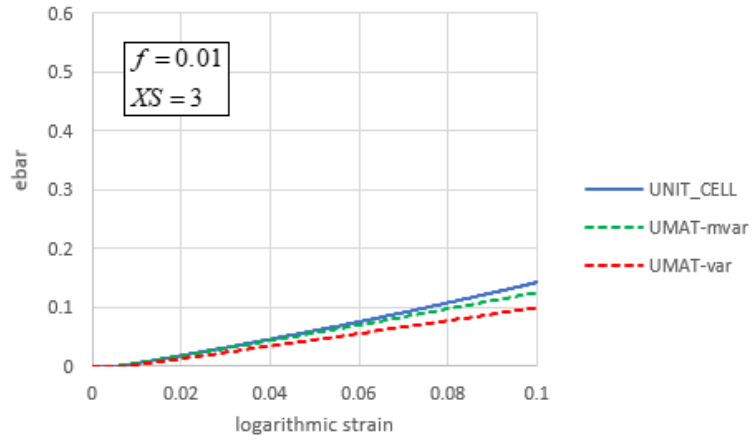

Figure 4.18: Equivalent plastic strain in the matrix for tension with initial porosity $f_0 = 1\%$ and triaxiality $XS = 3$

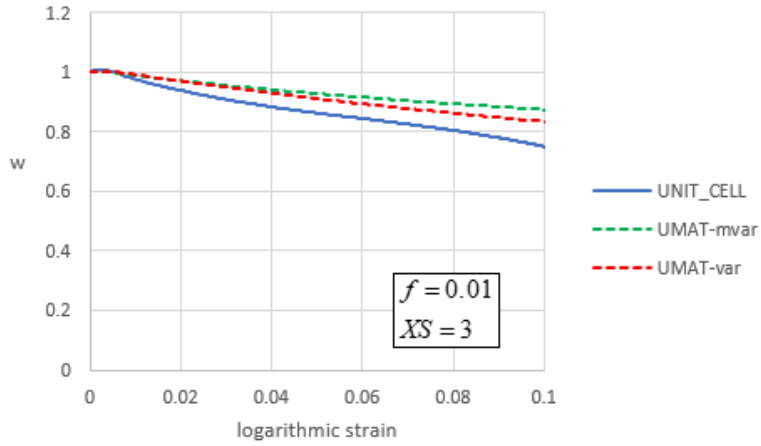

Figure 4.19: Aspect Ratio curves in tension for initial porosity $f_0 = 1\%$ and triaxiality $XS = 3$

4.3.3 $f_0 = 5\%$ initial porosity and Triaxiality $XS = 1$

Next, we study the problem of tension with initial porosity $f_0 = 5\%$ and triaxiality equal to 1. Regarding the stress-strain curves, both versions of the constitutive model deviate slightly from the results of the unit cell. MVAR model overestimates the stress while the VAR model underestimates it. Regarding the porosity, there seems to be an almost perfect match between the MVAR model and the unit cell calculations, while the VAR model underestimates the porosity. As far as the equivalent plastic strain is concerned, there seems to be a perfect match between the two versions of the constitutive model and the unit cell calculations. Finally, the MVAR model seems to predict more accurately the evolution of the aspect ratio.

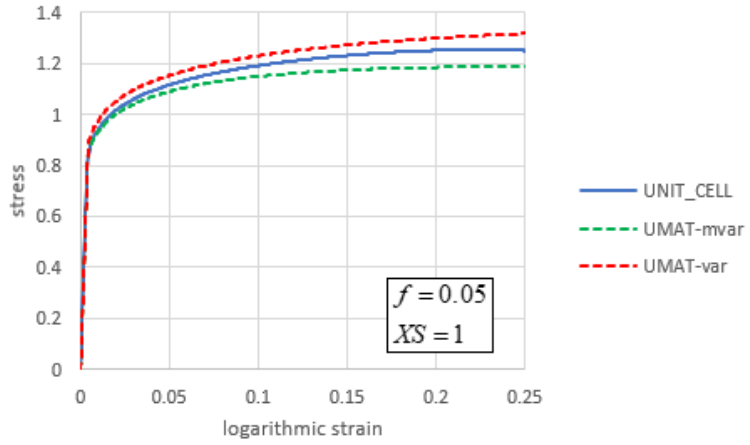

Figure 4.20: Stress-Strain curves in tension for initial porosity $f_0 = 5\%$ and triaxiality $XS = 1$

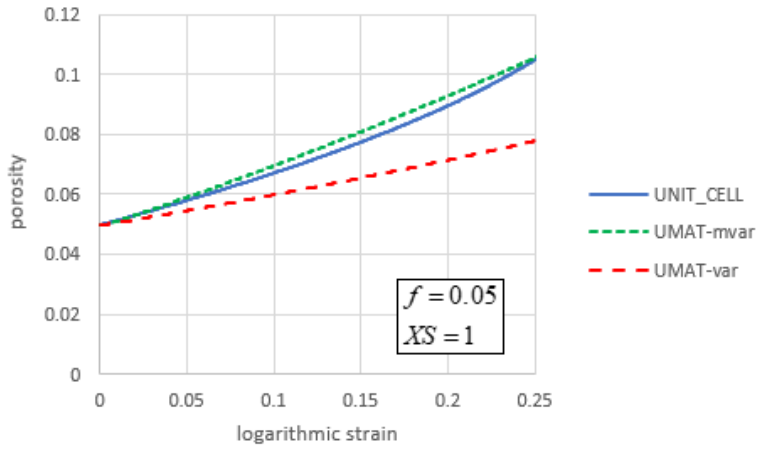

Figure 4.21: Porosity evolution curves in tension for initial porosity $f_0 = 5\%$ and triaxiality $XS = 1$

4.3.4 $f_0 = 5\%$ initial porosity and Triaxiality $XS = 3$

Finally, we study the problem of tension with initial porosity $f_0 = 5\%$ and triaxiality equal to 3. As we can see from the graphs below, the modified variational method predicts more accurately the stress-strain curve, the porosity evolution, and the aspect ratio. As far as the equivalent plastic strain is concerned, there seems to be a perfect match between the two versions of the constitutive model and the unit cell calculations.

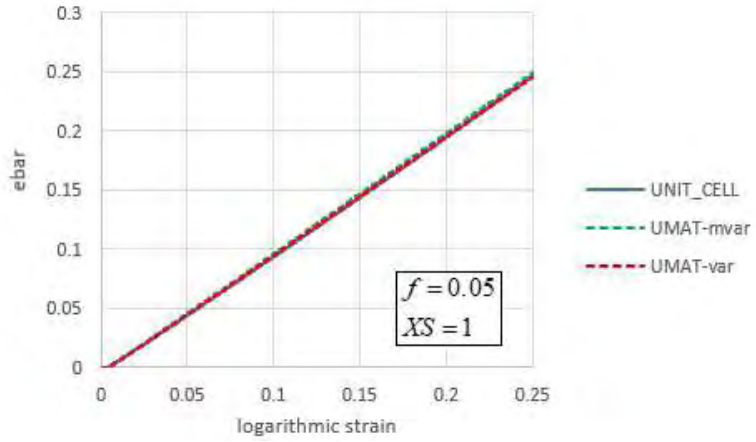

Figure 4.22: Ebar evolution curves in tension for initial porosity $f_0 = 5\%$ and triaxiality $XS = 1$

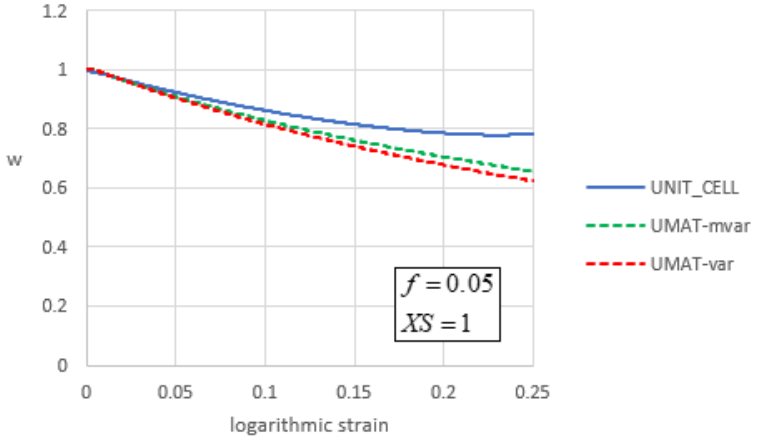

Figure 4.23: Aspect Ratio evolution curves in tension for initial porosity $f_0 = 5\%$ and triaxiality $XS = 1$

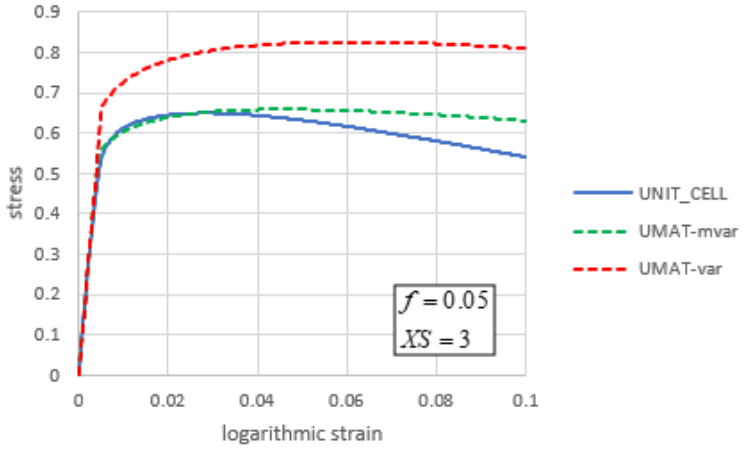

Figure 4.24: Stress-Strain curves in tension for initial porosity $f_0 = 5\%$ and triaxiality $XS = 3$

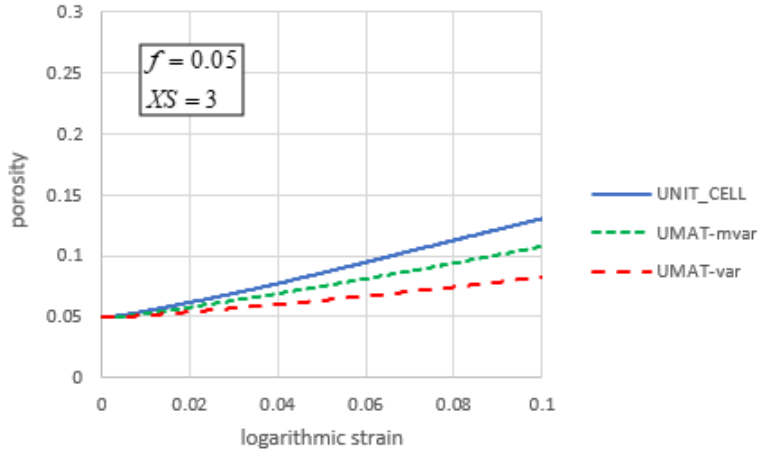

Figure 4.25: Porosity evolution curves in tension for initial porosity $f_0 = 5\%$ and triaxiality $XS = 3$

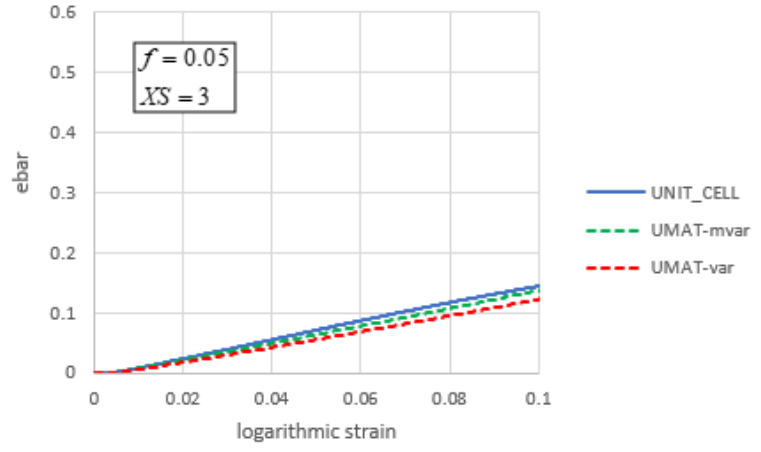

Figure 4.26: Ebar evolution curves in tension for initial porosity $f_0 = 5\%$ and triaxiality $XS = 3$

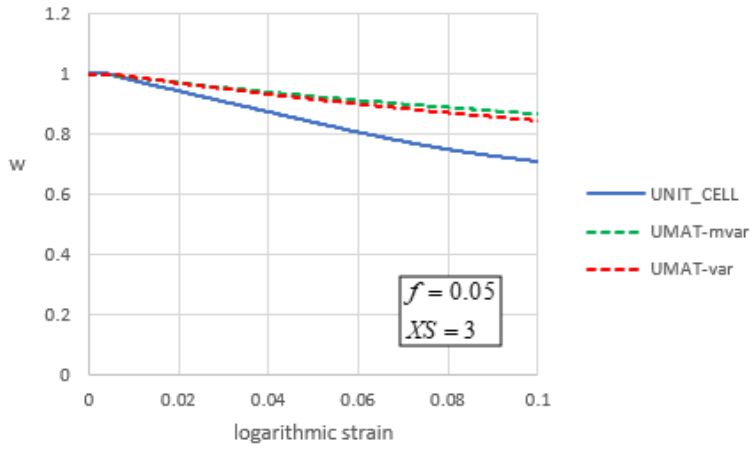

Figure 4.27: Aspect Ratio evolution curves in tension for initial porosity $f_0 = 5\%$ and triaxiality $XS = 3$

Chapter 5

Closure

5.1 General theory and Conclusions

The model that is developed here is a non-local version of the advanced anisotropic model presented by Ponte Castañeda and co-workers (Kailasam and Ponte Castañeda [13], Aravas and Ponte Castañeda [2]). Furthermore, there were changes in the numerical algorithm used, and the mathematical formulation in an attempt to improve the accuracy and the computational efficiency of the model.
As the original variational method was tested in numerous applications and loading conditions, it was observed that under high triaxiality loading conditions the solution was not matching the results from Gurson's model. Then the model was altered by Danas and Aravas ([7], [6]). The purpose of the modification was to give the VAR model the ability to attain the Gurson result in the purely hydrostatic limit.
In this Thesis we examined the accuracy of the MVAR model by studying the problems of uniaxial tension and tension under high triaxiality loading conditions with the initial porosity in the range $1\% \leq f_0 \leq 5\%$. The same calculations were conducted by using the MVAR and the VAR model and the predictions of the models were compared to unit cell calculations. So we reached the following conclusions:

Uniaxial tension
In the uniaxial tension the MVAR model seems to work well with the only drawback that overestimates the porosity. However, this overestimation does not seem to affect neither the stress-strain curve nor the evolutions of equivalent plastic strain and the aspect ratio. In general, the VAR model seems to work better in the case of uniaxial tension.

Triaxiality Control

- $f = 0.01$ and $XS = 1$: The estimation of porosity of the MVAR model seems to be inaccurate regarding the fact that is almost twice the prediction of the unit cell.Here the overestimation is critical and we can see that the stress curve is downgraded as a result of the weakening of the material characteristics caused by the excessive porosity. Whereas the porosity and the stress are not accurate, the equivalent plastic stain has a perfect match. As far as the aspect ratio is concerned, the MVAR model gives better

results.

- $f = 0.01$ and $XS = 3$: Under high triaxialities, the MVAR model describes more accurately the behavior of the porous material.
- $f = 0.05$ and $XS = 1$: Here we observe that, despite the not so high triaxiality, the MVAR model describes more accurately the behavior of the porous material.
- $f = 0.05$ and $XS = 3$: Once again, under high triaxialities the MVAR model gives more accurate results.

To recapitulate, the MVAR model works quite well under high triaxiality loading conditions, but in cases where both the porosity and the triaxiality levels are low the results generated are not accurate enough. An alternate modification needs to be implemented in the model in order to make the model perform better under low triaxialities. Also, the model we used is rate-***in***dependent. A rate-dependent version of the model could be developed in order to study dynamic problems such as the Charpy test. The unit cell used in this Thesis is a cubic unit cell with one pore in the center. An interesting future research would be to create unit cells with multiple voids and see if the results of the unit cell calculations change. Finally, we could introduce in the model a temperature dependence and simulate thermomechanical applications like the 3D printing of metallic materials.

Bibliography

[1] ABAQUS, Analysis User's Manual, Version 6.14, © Dassault Systémes, 2014.

[2] N. Aravas and P. Ponte Castañeda, "Numerical methods for porous metals with deformation-induced anisotropy", *Comput. Methods Appl. Mech. Engrg* **193** (2004) pp. 3767–3805.

[3] N. Aravas, Cartesian Tensors, *University of Thessaly Publications* (2005).

[4] D. Bigoni, Nonlinear Solid Mechanics Bifurcation Theory and Material Instability, *Cambridge University Press* (2012).

[5] Y.F. Dafalias, "The plastic spin", *J. Appl. Mech.* **52** (1985) pp. 865–871.

[6] K. Danas and P. Ponte Castañeda, "A finite-strain model for anisotropic viscoplastic porous media: I – Theory", *Eur. J. Mech. A: Solids* **28** (2009) pp. 387–401.

[7] K. Danas and N. Aravas, "Numerical modeling of elasto-plastic porous materials with void shape effects at finite deformations", *Compos. B Eng.* **43** (2012) pp. 2544–2559.

[8] R.A.B. Engelen, M.G.D. Geers, and F.P.T., Baaijens, "Nonlocal implicit gradient-enhanced elasto-plasticity for the modelling of softening behaviour", *Int. J. Plast.* **19** (2003) pp. 403–433.

[9] J.D. Eshelby, "The determination of the elastic field of an ellipsoidal inclusion, and related problems", *Proc. R. Soc. London A* **241** (1957) pp. 376–396.

[10] J.D. Eshelby, "Elastic inclusions and inhomogeneities", in: I.N. Sneddon, R. Hill (Eds.) *Progress in Solid Mechanics* vol. **II** (1961) pp. 87–140.

[11] A.L. Gurson, "Continuum Theory of Ductile Rupture by Void Nucleation and Growth: Part 1–Yield Criteria and Flow Rules for Porous Ductile Media", *J. Eng. Matl. Tech.* **99** (1977) pp. 2–15.

[12] M. Kailasam and P. Ponte Castañeda, "The evolution of anisotropy in porous materials and its implications for shear localization", in: N.A. Fleck, A.C.F. Cocks (Eds), IUTAM Symposium on Mechanics of Granular and Porous Materials, *Kluwer Academic Publishers* (1997) pp. 365–376.

[13] M. Kailasam and P. Ponte Castañeda, "A general constitutive theory for linear and nonlinear particulate media with microstructure evolution", *J. Mech. Phys. Solids* **46** (1998) pp. 427–465.

[14] M. Kailasam, N. Aravas, and P. Ponte Castañeda, "Porous metals with developing anisotropy: constitutive models, computational issues and applications to deformation processing", *Comput. Model. Engrg. Sci.* **1** (2000) pp. 105–118.

[15] J. Koplik and A. Needleman, "Void growth and coalescence in porous plastic solids", *Int. J. Solids Struct.* **24** (1988) pp. 835–853.

[16] W.M. Lai, E. Krempl, and D. Rubin, Introduction to Continuum Mechanics, *Butterworth-Heinemann* (1996).

[17] L.E. Malvern, Introduction to the Mechanics of a Continuous Medium, *Prentice-Hall Inc.* (1969).

[18] T. Linse, G. Hütter, and M. Kuna, "Simulation of crack propagation using a gradient-enriched ductile damage model based on dilatation strain", *Eng. Fract. Mech.* **95** (2012) pp. 13–28.

[19] J. Lubliner, Plasticity Theory, *Macmillan Publishing Company*, New York (1990).

[20] C.C. Chu and A. Needleman, "Void Nucleation Effects in Biaxially Stretched Sheets", *J. Eng. Matl. Tech.* **102** (1980) pp. 249–256.

[21] I. Papadioti, "Non-linear Homogenization Theories with Applications to TRIP Steels", Ph.D. Thesis., *University of Thessaly*, Greece (2016).

[22] I. Papadioti, N. Aravas, J. Lian, and S. Münstermann, "A strain-gradient isotropic elastoplastic damage model with J_3 dependence", *Int. J. Solids Struct.* **174-175** (2019) pp. 98–127.

[23] R.H.J. Peerlings, M.G.D. Geers, R. de Borst, and W.A.M. Brekelmans, "A critical comparison of non-local and gradient-enhanced softening continua", *Int. J. Solids Struct.* **38** (2001) pp. 7723–7746.

[24] R.H.J. Peerlings, L.H. Poh, and M.G.D. Geers, "An implicit gradient plasticity-damage theory for predicting size effects in hardening and softening" *Eng. Fract. Mech.* **95** (2012) pp. 2–12.

[25] P. Ponte Castañeda, "The effective mechanical properties of nonlinear isotropic composites", *J. Mech. Phys. Solids* **39** (1991) pp. 45–71.

[26] P. Ponte Castañeda and J.R. Willis, "The effect of spatial distribution on the effective behavior of composite materials and cracked media", *J. Mech. Phys. Solids* **43** (1995) pp. 1919–1951.

[27] A. Seupel, G. Hütter, and M. Kuna, "An efficient FE-implementation of implicit gradient-enhanced damage models to simulate ductile fracture", *Eng. Fract. Mech.* **199** (2018) pp. 41–60.